NTNU – Trondheim
Norwegian University of
Science and Technology

Bi-directional power converters for smart grids

Isolated bidirectional DC-DC converter

Welday Gebremedihn
Gerekial

Master of Science in Electric Power Engineering
Submission date: June 2014
Supervisor: Tore Marvin Undeland, ELKRAFT
Co-supervisor: Nils Backman(Dr.), Eltek company

Norwegian University of Science and Technology
Department of Electric Power Engineering

NTNU – Trondheim
Norwegian University of
Science and Technology

Galvanic Isolated Bidirectional DC-DC LLC Resonant Converter

Welday Gebremedihn Gerekial

Master of Electrical Power Engineering
Submission date: June 2014
Supervisor: Tore Marvin Undeland (Prof.)
Co-supervisor: Backman Nils

Norwegian University of Science and Technology
Department of Electric Power Engineering

Problem Description

Most activities in the world depend on the electrical power system so that uninterrupted power supply is needed. In most cases reliable power is stored in batteries. This can be expanded to supply the ac system by the same battery. This can be achieved by the application of power electronics with bidirectional power converters. Isolated bidirectional dc-dc LLC resonant converter is one of the building blocks that enable power to flow in both directions. The converter is static to be used in battery charging and discharging circuits for uninterruptable power supply, hybrid vehicles, space application, telecommunication, hospital etc.

LLC resonant converter is a promising alternative for converters to reduce switching losses and to improve the life time of the MOSFETs. LLC resonant converter reduce or eradicate the energy circulating in the converter by applying zero voltage switching and zero current switching.

The converter should be analyzed by simulation to the LLC resonant tank in the isolated bidirectional converter and also the efficiency of the bidirectional converter should be tested in the laboratory. Develop the automatic controller, small signal analysis and minimize the loss by selecting the proper resonant value. If time, the converter should be developed and tested on laboratory.

The goal of the thesis is to minimize the switching loss of the MOSFETs by adding the LLC resonant tank on the isolated bi-directional dc-dc converter and also improve the lifetime efficiency of the converter. In addition to develop LLC resonant tank in the isolated bidirectional converter also develop automatic bi-directional controller.

Assignment: Trondheim 10.01.2014
Supervisor: Tore Marvin Undeland(Prof.)
Co-supervisor: Backman Nils

Abstract

As part of my master thesis I have take part in Isolated Bidirectional DC_DC LLC resonant converter from Eltak company. Application of power exchanges takes place in either direction using two unidirectional DC-DC converters. Even though it is common to use power flow in unidirectional, but later due to many application growing emphasis on small size, compact the two unidirectional way of power flow and efficient power systems. This gives increasing interest to develop a bidirectional type of power flow with bidirectional converter. This is especially for DC power application like motor drives, uninterruptible power supplies(UPS), alternate energy system, telecommunication, space technology, hybrid Automotives, battery charger and battery discharger.

After a literature study of different types of converter topology , the isolated bidirectional DC-DC LLC resonant converter has been selected. This resulted in LLC resonant tank have for both mode of operation. The converter is dual active bridge with isolated high switching frequency transformer. The bridge on the high side is voltage-fed and current-fed on the low side of the converter.

Since the isolated bidirectional DC-DC converters have the capability to perform the bidirectional power flow in a compact form or a single device to perform such application. Therefore for this specialization project it is proposed to have dual full-bridge isolated bidirectional DC-DC LLC resonant converter in a compact and single device converter. The topology computable for this type of isolated bidirectional DC-DC converter. In this bidirectional converter mainly discussed about the role LLC resonant arrangement instead of PWM for reducing power loss in high switching frequency.

Acknowledgements

I would like to express my gratitude and appreciation to my supervisor Prof. Tore Marvin Undeland for his constant encouragement, guidance and support during whole period of time stay on NTNU for the thesis and other supporting courses.

I would like also to thank to my co-supervisor Dr. Backman Nils for his guidance and excellent participation in topology selection and further discussions on different specifications. He was also committed for supporting in lab work by send some lab components.

Furthermore, I would like give my appreciation to ELKRAFT power electronic lab staff members for their open welcome to help in laboratory equipment arrangement. I would like appreciate my colleague master student for creating pleasant work environment at the reading room.

At the last I would like to gratitude thanks my wife and my close friend for their support during my study.

Table of Content

List of Figures

Chapter 1-Introduction

1.1 General Introduction

The world now is going to exercise the power electronic applications device for complex systems when most difficulty face for human being in many stream of fields. Over the last three to four decades power efficiency become the main concern of researches for power conservations as a result these leads to grow compact power supplies grows significantly. Power electronics circuits primarily process the energy supplied by utility or storage devices to a form which matches with required load or storage device through the application of semiconductor devices to control the voltage and current values . The energy can supplied from utility grid or bank of batteries; with the application ranging from high power conversion equipment of MW to the very low power equipment of a few watts.

Most of power converter devices have common unidirectional application with power being supplied from the source to the load. However different types of applications require dual direction; the applications such as motor drives, uninterruptible power supplies(UPS), alternate energy system, telecommunication, space technology, hybrid Automotives, battery charger and discharger etc. require using another system of conversion which is not similar to unidirectional. Therefore these applications introduce power converter with bi-directional power transfer property.

Conventionally, the two independent unidirectional converters can be used together parallel for achieving bi-directional power transfers. Bidirectional DC-DC converters recently gates awareness due to application of bidirectional power transfer between different dc sources buses. The demand for development of complex, compact and efficient power system implementation has encouraged scientists in bi-directional converter development.

1.2 The Art of Bi-Directional DC-DC Converter

1.2.1 Introduction to Bidirectional dc-dc converter

Most bidirectional DC-DC converter topologies can be illustrated as block diagram shown in the Fig-1.1 below and it also characteristics power flows in both directions[1-3]. Energy storages in general uses bidirectional DC-DC converter for charging and discharging applications may be either in half-bridge or full-bridge arrangement of semi-conductor switching devices. The buck type of converter has energy storage on the high voltage side, whereas boost type of converter has energy storage on the low voltage side.

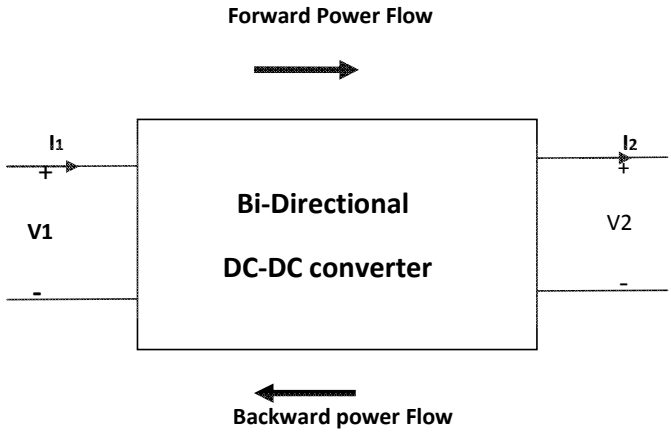

Fig.1- 1 Illustration of bidirectional power flow

The concept of power flow in both direction for bidirectional dc-dc converter is operation of switching devices realize current flow in each way. Bidirectional dc-dc converters are developed from two unidirectional semiconductor switching devices such as; MOSFET, Transistors and IGBT power switches constructed with parallel diodes. These parallel diodes serves double sided power flow. Even though there are many topologies of bidirectional dc-dc converter; basically they are divided into two types such as an isolated bidirectional DC-DC converters and non-isolated bidirectional DC-DC converters based on the isolation material between input and load[4-6].

1.2.2 Non-isolated Bidirectional DC-DC Converter

Non-isolated bidirectional DC-DC converters power flow without any isolation between input and load[7]. The transformer-less non-isolated dc-dc converters can be either boost, buck or buck-boost converters. Even though it's attractive to obtain isolation[8-9] for high frequency conversion applications between the load and the source but non-isolated type of converter is more attractive from the efficiency, size, weight and cost point of view.

The most familiar DC-DC converters, such as buck and boost converters have only one direction power flow. Since step-up and step-down converters contain diode on their structure which has characteristic of one direction power flow. However it has advantageous to change unidirectional converter into bidirectional by replacing the diodes with controllable switches like MOSFETs and IGBTs. As Fig.1-2 shows that the structure of converter is a combination of two unidirectional step-up and step-down converters. So that the unidirectional converters are transferred into bidirectional converters by replacing the diodes with controllable switches like MOSFETs and IGBTs [10] shown in unidirectional dc-dc converters.

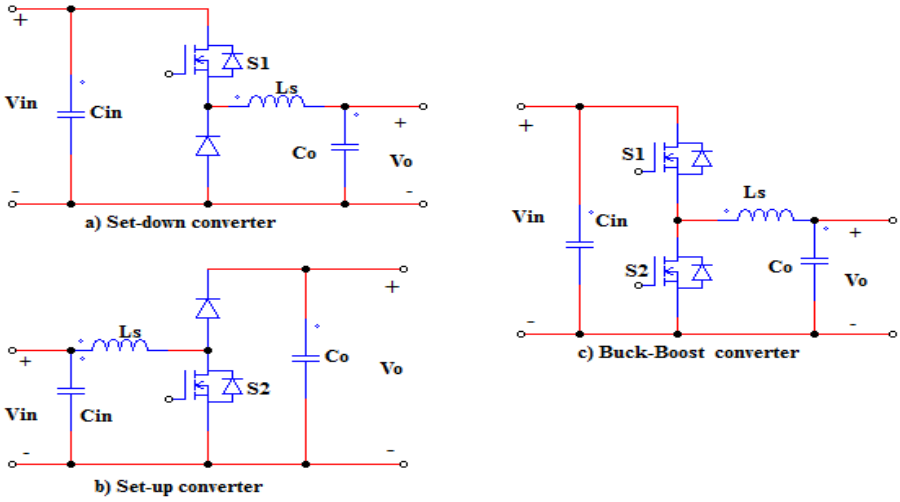

Fig.1- 2 Constructing non-isolated bidirectional DC-DC converter from two unidirectional converter

Some of the limitations relating to the Non-isolated bidirectional dc-dc converter compared to isolated bidirectional dc-dc converters shown in the above Fig.1-2 are:

- It can only operate boost mode in one direction and buck mode in the other direction. This means the voltage duty ratio(D) , which is defined as $D = V_o/V_{in}$, is either smaller than one or equal to one in one direction. This indicated the voltage level of dc-dc converter is determined by the arrangement of the switch device and filter devices.
- When the voltage ratio become very large this shows not practical.
- Due to lack of galvanic isolation between the two sides of the network if a short circuit risk happened on one side of the system; the whole system of the DC-DC converter will be failed.

1.2.3 Isolated Bidirectional DC-DC Converters

The transformer is used for isolating bridge converters which is on both sides of DC-DC converters or it isolates input and load. While the transformer has additional cost in addition to the component cost; however it has critical component for isolating the source and load by providing impedance matching between the two sides and prevent a short circuit occurred on one side of the enter system. Isolated bidirectional DC-DC converters can be classified as full-bridge, a half-bridge or push-pull bidirectional converters[11-12] based on the arrangement of the switching devices and their application.

Generally bidirectional converters have a structure similar to the Fig. 1-3. The topology consists of two high switching frequencies DC-AC and AC-DC converters with similarly high frequency transformer which is primarily used to maintain the galvanic isolation between the sources. Therefore the topology consists both rectifier and inverter on either of its bridges. Since the transformer has a numbers of turns on both sides then it is essential for voltage matching between the two sources. As an energy is transferred in either direction is required for the enter system, therefore each side of the converter must have a capability to transfer in both direction using controlling system.

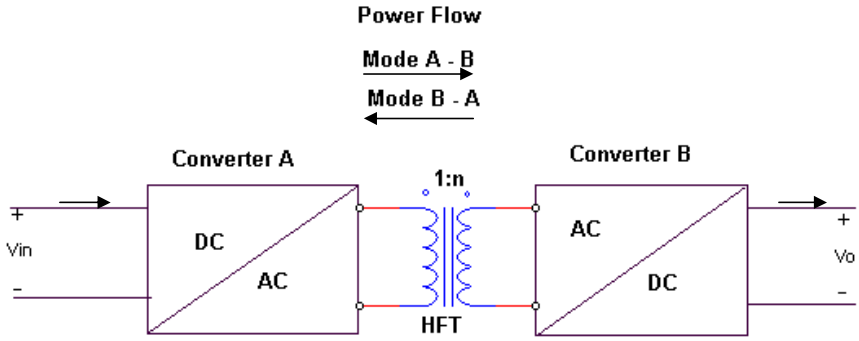

Fig.1- 3 Basic structure of isolated bidirectional DC-DC converter

As the term bi-directional indicates, there are basically two mode of operations where th of switches either turned-off or turned-on in order to control power flow from either d As Fig.1-3 shows the two mode of operations are noted as charging/step-down and disc step-up detail will be discussed in chapter-3. Notification of the power transfer can be dif publication to publications. There are different isolated bidirectional dc-dc c publications[20-22].

1.3 The Need For Galvanic Isolation

Transformer isolation needs for a system when there is no need of direct connection source and load. If there is no an isolation between the load and the source, a single circ occurred on any circuit component of the system has high probability to damage th system. If two fault develop anywhere in the system, a current path will exist among faults therefore a short circuit occurred on the converter. For this case it need to either t a controller or add transformer isolation device in order to interrupt power system during minimize the current due to the fault which damage components before the protective co functions are activated. But if we place the isolated galvanic components between the so load then these problems and faults can be minimized even eradicated the fault at all. T system will remain powered-on and not damaged the system entirely. Current fault path happened if there are multiple faults on one side of the isolation zone. It is therefo advantageous to have galvanic isolation for almost all loads. Fig.1.4 shows the above e either we have galvanic isolation or not, X indicates there is a fault on the short circuit ar

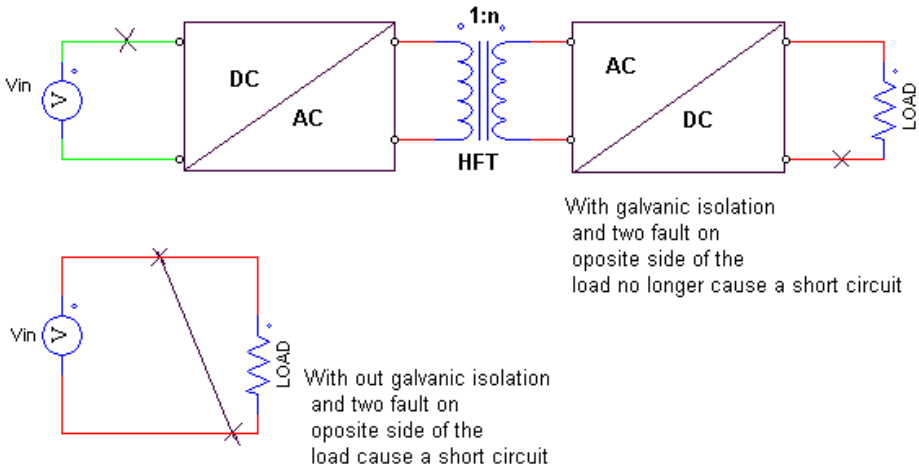

Fig.1- 4 Effect of galvanic isolation in circuit.

1.4 Literature Review

The first step towards maximizing the performance of isolated bidirectional DC-DC converter is to review the limitation of the existing systems. These converters were the focus of significant research interest over the last four ten years. In this section, previous works in the area of bidirectional DC-DC converter is reviewed with the objective of current and voltage status of research in this specialization project evaluating topologies for their possible implementation in low power LLC bi-directional DC-DC converters.

1.4.1.High power bidirectional dc-dc converter

Various topologies variations for DC-DC converters of high power applications with bidirectional power transfer have been proposed and developed through the last four decades. For the development of the efficient power, dc-dc converter they use either resonant[13], soft switch achieved by controlling phase shift [14-16], or hard pulse width modulation(PWM)[17]. Even though PWM and soft switched achieved by controlling phase shift converters have their own advantages but they have also limitations to use for middle power bidirectional dc-dc converters. These converter topologies aren't efficient to use for middle bidirectional dc-dc converters due to the following drawbacks;

- large number of switches
- large components
- limited range of satisfactory for high frequency
- complex power and control circuit etc.

Operation of the converter in series resonant converter[13] is seen as high power densities and has the advantage of natural commutation and soft switching ability. However they have limitations in terms of frequency sensitivity, higher voltage and current stresses in the devices of the topologies and large ripple currents in the output and input capacitive filters. Resonant converters also require careful selections for matching the operation frequency of the resonant tank circuit, and magnetic saturation.

The dual bridge presented [14] achieves lower switching losses by controlling the phase shift between the two inverting stages operating at high frequency. It uses the leakage inductance of the transformer as the main energy transfer component. At high level power and frequencies design and implementation of transformer and controlling the leakage is extremely complicated[14].

1.4.2 Medium and low power bidirectional dc-dc converter

As a high power applications, medium and low power bidirectional dc-dc converters are based on either hard switching[16], soft switching or resonant switching type[19]. Most of these dc-dc converters are well suited for a particular application even though they have their own drawback. Their limitations can be described as;

- lack of isolations
- high component stresses
- large ripple current through the filtering inductors
- at high frequencies the converter designed to operate under resonance and soft switching may suffer from hard switching of the devices.

The converters operating in the resonance modes[19] have the limitation on the load and voltage conditions and also subject the devices to high stresses. The presence of only one active switch in the circuit path during each direction of power flow leads to a higher rate for the switch and component as a whole results increase cost. In addition conduction losses in the resonant part also increase due to their series arrangements. The bidirectional converter topology designed in [19] does not provide galvanic isolations between the battery and the load or source which is often required in battery operated power systems.

1.5 Thesis Structure outlines

This thesis is organized as follows:

Chapter 1 gives a general over view on different bi-directional DC-DC converter and give the application of different bidirectional topologies in DC-DC converter. In general DC-DC converters are classified as isolated and non-isolated bi-directional. Bi-directional DC-DC converters can be constructed with a series of two-stage DC-DC converter with an isolation of transformer between them. The selected topology for this dc-dc converter is isolated bi-directional dc-dc LLC resonant converter.

In **Chapter 2** gives an over view of three type of resonant converter arrangement. The chapter also detail discuss about each arrangement about their advantage and disadvantages. Based on the application of these resonant converters the most efficient and serve for reducing circulating energy within the converter is LLC arrangement of the resonant tank.

Chapter 3 presents detailed components of the dual full-bridge bi-directional DC-DC LLC resonant converter. This also includes the circuit and simulation results for both operation modes; that is charging mode of operation and discharging mode of operation. Charging mode of operation gives more detail in step-down and the discharging also deals with step-up from the battery or other source to the main grid. This chapter also includes design of the digital circuit for MOSFET gate drive signal controller. Efficiency of isolated bi-directional DC-DC resonant converter is almost 97%.

Chapter6 discuss the small signal analysis and develop the controlling system of the converter and in addition drive the transfer function of the plant and the system. The controller type also selected.

Chapter5 The capacitor filter design and calculated the capacitor value based on the specific ripple factor Rp. Also design the gate driver and the bootstrap-of the controller.

chapter 6 describe the experimental result of the converter for forward and backward mode of operation.

Chapter 2- LLC Resonant Converters

2.1 Introduction

High power, efficiency and density are the major core cause for the development of new resonant converter. These converters are called LLC resonant converters which solve the drawbacks of the previously known series and parallel resonant converters will discuss in detail in this chapter. Based on their fusibility, these resonant converters developed due to their ability of higher switching frequencies, higher efficiencies, simple and small packaging. These are also the paths considered for the development and manipulating of the LLC resonant converter[23]. Within all these issues a topology capable of higher switching frequency with higher efficiency will be achieved. The goal of resonant converter is solving the limitation of the hard switching and PWM switching that produces high loss will be minimized to a very small value.

The most earlier resonant converter which was investigated mostly around three decades ago [23-24], but later the power loss faced in DC-DC converters were resolved due to the implementation of these resonant converter topologies to operate at high switching frequencies. In general traditional trend of resonant converter topologies can be classified into three major classes. The classification is based on the arrangement of the resonant components; Series Resonant Converter, Parallel Resonant Converter and Series Parallel Resonant are the three most popular topologies.

2.2 Three Most Common Resonant Topologies

2.2.1 Series Resonant Converter

In this case, the dual active full-bridge switch topology is connected to the series resonant converter on both sides of the transformer as shown in the Fig.2-1. The resonant inductor Lr and Resonant capacitors are series connected with active full-bridge MOSFETs switches . They form a series resonant tank which is serially connected to load so that the resonant tank and load are voltage dividers where as the load is reflected from secondary to the primary side of transformer. It is possible to control the impedance of the resonant tank by varying the switching frequency of input voltage.

Since the impedance of the resonant tank and loads are voltage divider, the gain of the voltage ratio or voltage gain to this type of resonant tank is always less than one. At resonant frequency impedance of the series resonant tank will be insignificant and as a result the voltage drop across the resonant is not considered in the analysis. Therefore at the resonant switching frequency the voltage gain almost have unity value.

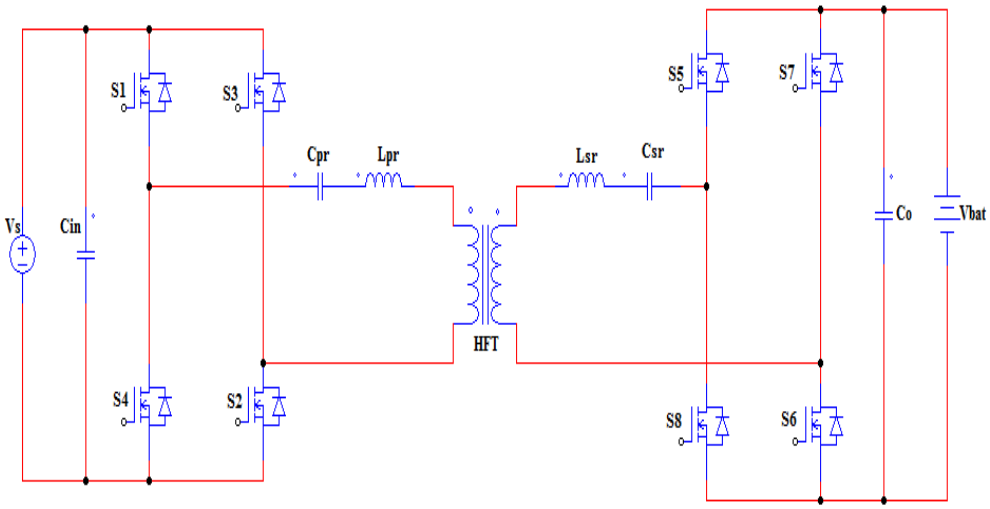

Fig.2- 1 Full-bridge series resonant converter

The general code developed in appendix[A1] generates value for the parameter of the resonant tank(i.e. L_p, C_p, L_s, and C_s). The developed code interface with simulink developed plant output voltage and switching frequency. The generated values of the resonant tank parameter value are selected if they satisfay the required resonant frequency. From Fig.2-2 the parameter values are L_p = 335.8µH, L_s = 28.8µH, C_s = 392nF and C_p = 13.5µF.

The parameters value for this series isolated bi-directional resonant converter are specified as follow:

Transformer turn ratio: 25:3

Input voltage: 400V

R_{load} : 0.8Ω

Resonant frequency: 100KHz

From Fig.2-2 selecting the appropriate value of the resonant parameters from the right side of the resonant frequency is recommended operating regions of the resonant tank to have high efficiency. For high efficient resonant converter the loss is consider for the selection of the operating region, so that zero voltage switching region is the appropriate range. This is due to the law loss during zero voltage switching(ZVS) and MOSFETs application in DC-DC converter. If the region selected for the operation is on the left side; then the switching frequency is lower than the resonant frequency the converter will work under zero current switching(ZCS) condition.

From Fig.2-2 characteristic of DC-gain, the DC gain slope is negative then the converter is under zero voltage switching condition, but when the DC gain slope is positive the converter is under the condition of zero current switching. But due to the internal structure of the MOSFET is advisable to operate the resonant converter under the ZVS region. Referring to Fig-2.2 the operating region for small load implies high switching frequency in order to have a constant output voltage. This is a main drawback and limitation for the SRC.

Based on the above analysis SRC is not appropriate structure of the resonant tank for DC-DC converter. Its main limitations are: in light load regulation and high circulating energy.

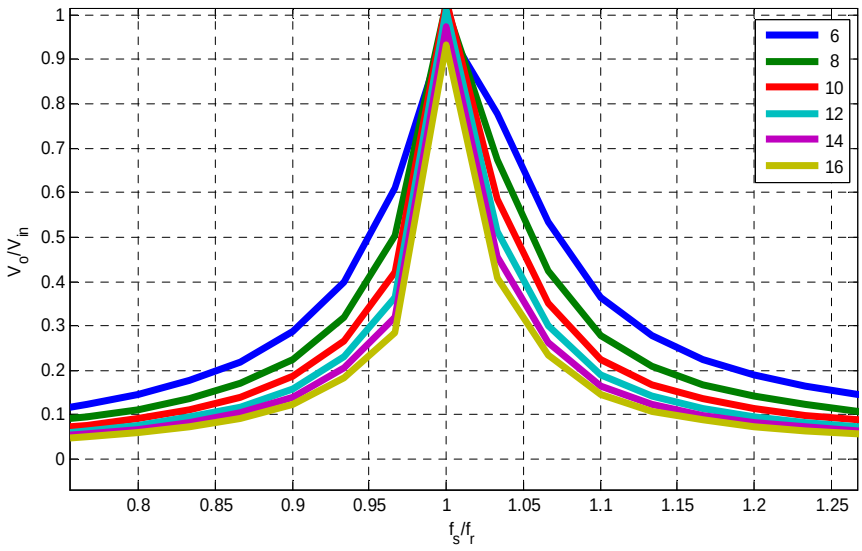

Fig.2- 2: DC-gain characteristics of SRC resonant converter

2.2.2 Parallel Resonant Converter

The schematic circuit diagram for the PRC is shown in the Fig.2-3 and the arrangement of the capacitor and inductor are still similar as described in SRC, when they are compared with the arrangement of resonant tank components. The only difference is the arrangement of capacitor with load, where capacitor in parallel resonant converter is parallel to load but series in series resonant converter. More familiar names for this converter can be called as a series resonant converter with parallel load impedance.

As described in the series resonant converter the general code developed in appendix[A2] generates value for the parameter of the resonant tank(i.e. L_p, C_p, L_s, and C_s). The developed code interface with simulink developed plant output voltage and switching frequency. The generated values of the resonant tank parameter value are selected if they satisfay the required resonant frequency. From Fig.2-4 the parameter values are

$L_p = 543.8\mu H$, $L_s = 12.8\mu H$, $C_s = 4522nF$ and $C_p = 225\mu F$.

The parameters value for this parallel isolated bidirectional resonant converter are specified as follow:

Transformer turn ratio: 25:3

Input voltage: 400V

R_{load} : 0.8Ω

Resonant frequency: 100KHz

The dc-gain characteristic of the resonant converter is shown in Fig.2-4. As shown in the figure the dc-gain characteristic(Q) of the PRC is ranging from 4 to zero.

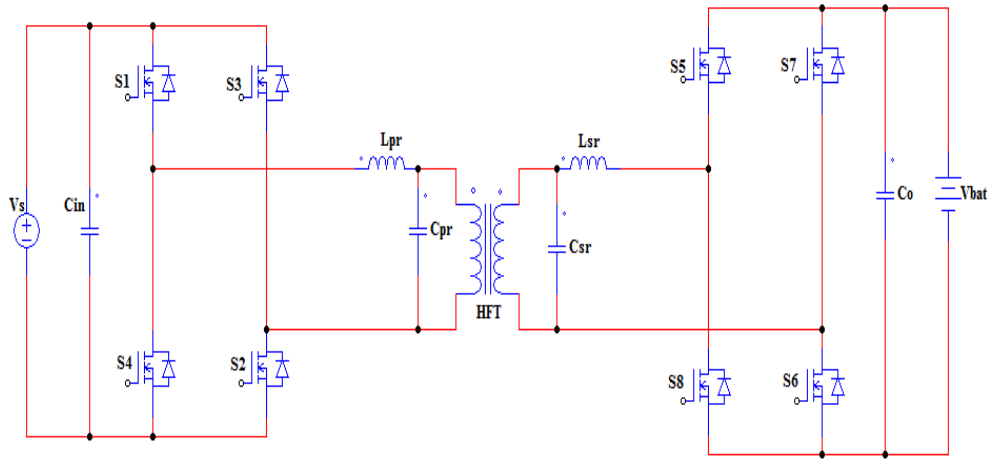

Fig.2- 3: Full-bridge parallel resonant converter

As shown on Fig.2-2 in the SRC operating region is very narrow with small load but the switching frequency is very high and make difficult to have almost constant and regulated output voltage. But PRC has a wider operation region with light load and very small switching voltage variation. Therefore it has an advantage to have constant and regulated output voltage. At high input voltage the converter is working at higher frequency even far away from the resonant frequency values.

PRC still faces some limitations in circulating energy which occur during small load. So that the load is parallel with resonant capacitor in the input side of the isolation part with small value impedance even at no load condition. Even though parallel resonant converter have better range of operation but still have the above limitations. Therefore Parallel resonant converter is not preferable similar to series resonant converter in dual active full-bridge bidirectional DC-DC converter and this lead to another alternative option to solve the limitation.

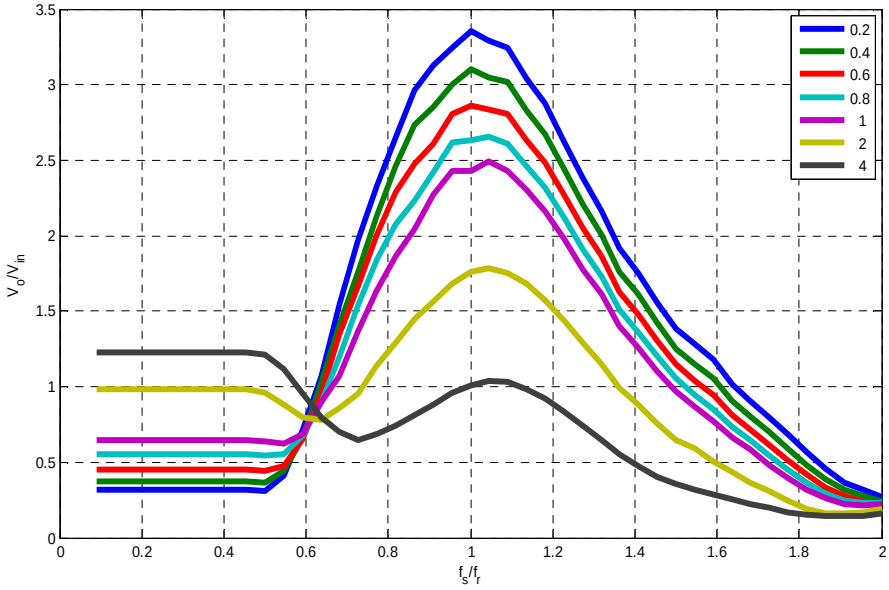

Fig.2- 4: DC-gain characteristics of PRC resonant converter

2.2.3 Series Parallel Resonant Converter

SPRC merges the above two resonant topologies together and its resonant bank consists of three components, such as series resonant inductor(Lr), series resonant capacitor(Csr) and parallel resonant capacitor(Cpr). Its schematic diagram is shown in the Fig.2-5. The resonant tank of SPRC is constructed from both structures, series resonant converter and parallel resonant converter. This combination leads to minimize the limitation in each resonant topology separately. The Combination of these two structures of SPRC can regulate the output voltage even at no-load conditions.

The dc-gain characteristic(Q) of the series parallel resonant converter is mirror of the LLC resonant converter which will see in detail in the next section of this chapter.

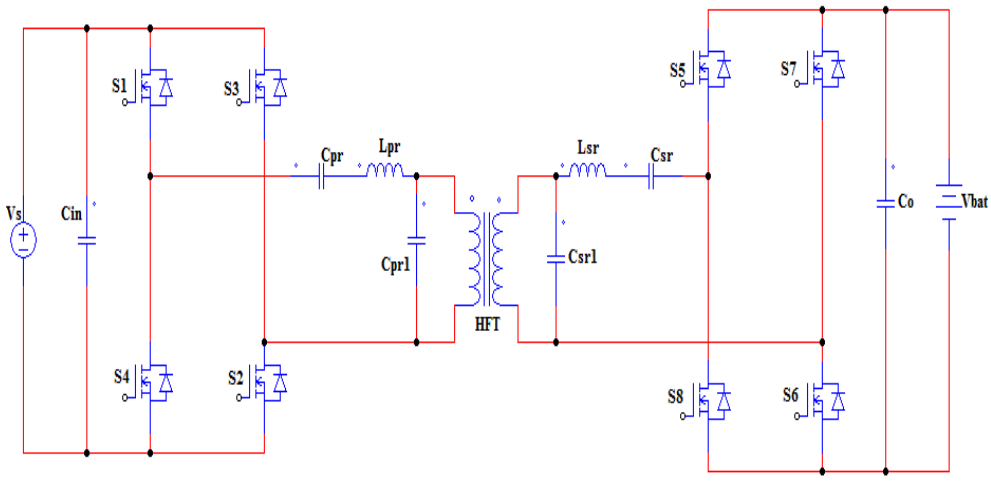

Fig.2- 5: Full-bridge series parallel resonant converter

As discussed in the two different topologies above; they have a circulating energy and turn off-current for switches (in this case MOSFETs) face drawback at high input voltage. Even though SPRC arrangement structure of the capacitor and inductor reduce the problems on one but not for the second, still it has a high conduction loss and switching loss at wide input voltage. While SPRC has limitation of wide range input voltage design; In this wide range of voltage input the conduction loss and switching loss will dramatically increase at high input voltage, so the switching loss is very approach to PWM converter at the same level input voltage.

Then it is possible to generalize based on the above drawback of designing on SRC, PRC and SPRC difficult to optimize at high input voltage due to high conduction loss and switching loss. So that, to achieve high switching frequency and higher efficiency researchers developed another type of topology called LLC (resonant Inductor, resonant capacitor and magnetizing inductor)[28].

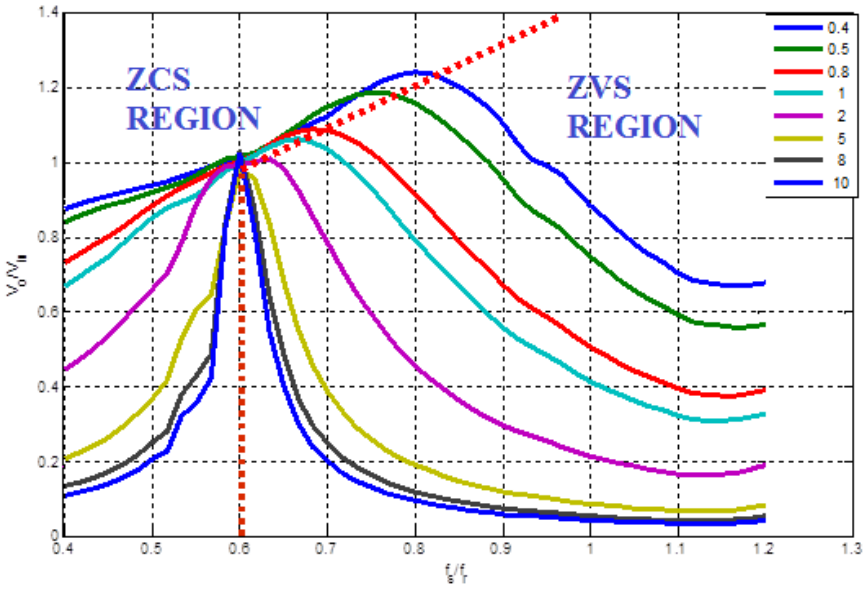

Fig.2- 6 : DC-gain characteristics of SPRC resonant converter

2.3 LLC Resonant Converter

The above three traditional resonant topologies have many limitations during the high voltage input. Their main limitations are high circulating energy and large switching loss which are occurring during the high voltage input. From Fig.2-7 LLC resonant can be designed by interchanging the position of the L to C and C to L from LCC arrangement of inductor and capacitors in series parallel resonant converter. Here there are two resonant frequencies: Lr and Cr determine the higher resonant frequency and the lower resonant frequency which is determined by the series combination of inductance Lr and Lm with Cr[28].

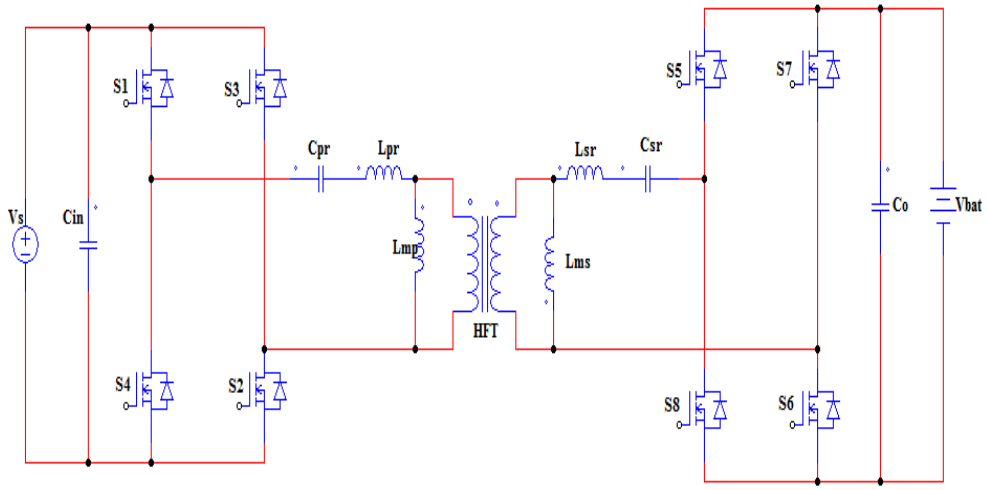

Fig.2- 7: LLC resonant converter topology

Even though the LLC resonant converter existed for a very long time, its lack of understanding of the characteristics of the converter helps to serve as a series resonant converter with passive load. In other words it is designed to operate at switching frequency which is much higher than the resonant frequency of the series resonant tank of Lr and Cr; but in series and parallel resonant converter switching frequency is equal to the resonant frequency. Advantages of LLC resonant converter compared to the above three traditional resonant converters has a narrow switching frequency range with light load and ZVS capability with even no no-load.

2.4 Operation of LLC resonant converters

LLC resonant converter have zero voltage switch(ZVS) and zero current switch(ZCS) regions of DC characteristics as shown in the Fig.2-7. For LLC resonant converter have two types resonant frequencies due to parallel arrangement of one inductor; one is determined by the resonant components of Lr and Cr and the second type of resonant frequency is produced due to Lm and Cr. The frequencies can be analysis as the following equations:

$$fr1 = \frac{1}{2\pi\sqrt{LrCr}} \quad (1)$$

$$fr2 = \frac{1}{2\pi\sqrt{(Lm+Lr)Cr}} \quad (2)$$

"LLC DC characteristics is sketched and analyzed , take samples for 400V input operation; it could be placed at the resonant frequency of f_{r1}, which is the resonant frequency of the series components of the LLC resonant converter(i.e. Lr and Cr)[25]. As shown in Fig.2-8 low switching frequency and large DC characteristics are obtained as input voltage decreases.

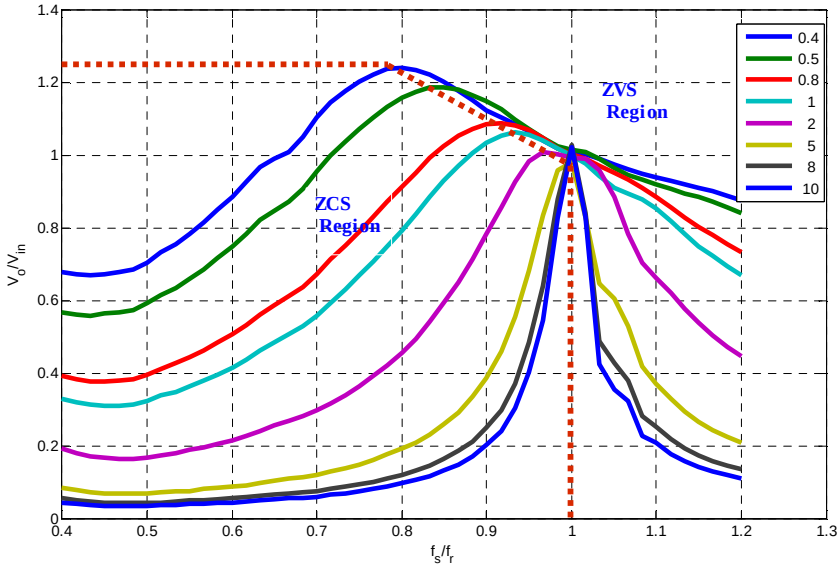

Fig.2- 8: DC characteristics of LLC resonant converter

2.5 System Optimization For LLC Resonant Converter

The practical results show that PWM converters have drawback to achieve high efficient and large operation ranges. The LLC resonant converters solve the drawback of PWM due to exhibit of high performance in small voltage stress and low switching loss on rectifier side of the converter and this results lead to have higher efficient than PWM converter.

2.5.1 Improve MOSFETs Selection For High Frequency Resonant Converter

For high-voltage MOSFET's, it is better to select high quality switches such as super-junction MOSFETs which offers low R_{ds}. Infineon's CoolMOS have such quality for low switching loss and high efficiency[29]. It is necessary to discuss the performance of the convectional MOSFET's in this application before deciding to use Infineon CoolMOS in LLC resonant converter.

Under low-load situation the switches become unable to fully recover, therefore large recovery current can cause the switches to breakdown and lead the failure of the system. The unique Infineon MOSFET quality is to overcome these unable recovery in low load using its internal intrinsic diode structure of switches. The special property of Infineon super-junction MOSFET's solve the conventional drawback in low-load reverse current by applying different path for the reverse current[30]. Even though the failures is recovered by the MOSFET's intrinsic diode property, but the reverse recovery current drops the efficiency of resonant converter.

Since the current through the convectional switching device and the reverse voltage are very small , this lead the MOSFETs to fail in the primary full-bridge side. This small reverse voltage is not sufficient for the conduction of the within this short conduction period. Since in super-junction MOSFETs the P-doped column is added to the N-epi region, the P-column serves as balancing the charge at the conduction channel and this gives the device to have high concentration of doping with the same blocking voltage[29,31]. The higher concentration of doping in N-epi leads high conduction or low on-resistance in the super-junction MOSFETs. The P-column serves to have enough time for reverse current flow and solve the drawback of the convectional MOSFETs in reverse current leads to failure of the device.

2.6 Operation principle of LLC Resonant Converter

As described in the above sub-sections LLC resonant converter topology has reduced magnetizing inductance than the series and parallel resonant converter. The less magnetizing inductance in LLC resonant realize soft switching for the primary side switches. As shown in Fig.2-10 dc-voltage characteristic gain can be grater or less than one. From these voltage gain curves, the switching frequencies are normalized by the resonant frequency which is developed in chapter-4 and represented as:

$$fr = \frac{1}{2\pi\sqrt{LrCr}}$$

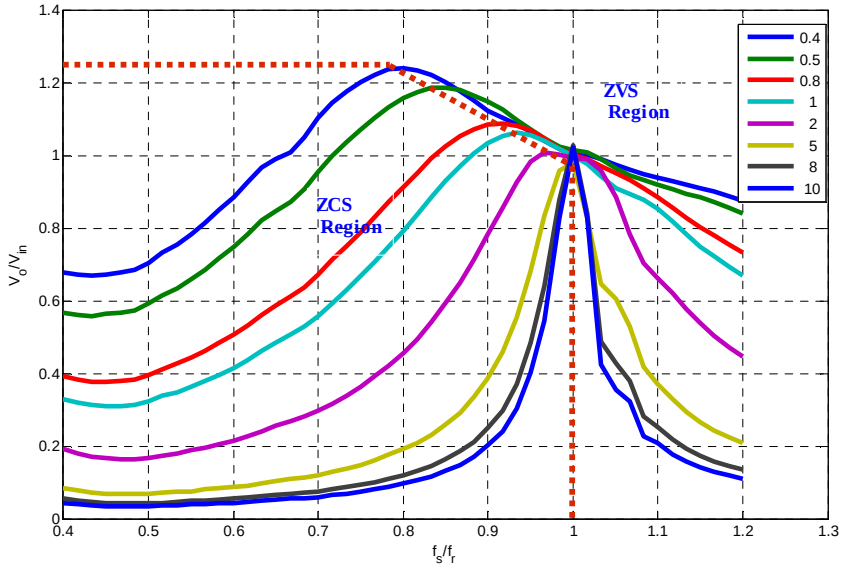

Fig.2-10 dc-voltage gain characteristic for LLC resonant converter

From Fig.2-10 due to its different probability operation of LLC resonant converter, it is complex to gate the operational frequency of the converter. This happened if the converter haven't controlling feedback from the output. According to switching frequency of the LLC resonant operation can be classified as above, below and equal to resonant frequency[32, 33].

The general code developed in appendix[A3] generates value for the parameter of the resonant tank(i.e. L_p, L_{mp}, C_p, L_s, L_{ms}, and C_s). The developed code interface with simulink developed plant output voltage and switching frequency. The generated values of the resonant tank parameter value are selected if they satisfay the required resonant frequency. From Fig.2-10 the parameter values are:

$L_p = 6.5\mu H$, $L_s = 93nH$, $L_{mp} = 71.5\mu H$, $L_{ms} = 1\mu H$, $C_s = 27.25\mu F$ and $C_p = 391nF$.

The fixed value are similar to the series and parallel resonant converter as defined above.

2.6.1 Switching Frequency equal to resonant frequency

Series and parallel resonant converter are operated where resonant frequency equal to switching frequency increase the efficiency of the converter as described in the above sub-section. Furthermore the magnetizing component of the resonant converter modifies the voltage gain characteristic. In SRC and PRC, the ZVS operation region ensures for designing margins during design stage, however the converter is an able to operate at this operational region.

In LLC resonant converters, ZVS region has not limitation of operation. Therefore ZVS can be achieved for any switching rages that is either higher or lower than the resonant frequency. Here in LLC resonant converter no need of designing for margin, so that the converter can be operated with resonant frequency to achieve high efficiency for the converter.

When the switching frequency is equal to the resonant , the converter has achieved zero voltage switching for the primary full-bridge sides. However the switches turn-off current has very high magnetizing inductor current. These high switching magnetizing current can be reduced by choosing suitable magnetizing inductor, which reduces turn-off losses. Two of secondary full-bridge intrinsic diodes are either turned-on or turned-off with low di/dt. This refers the intrinsic diodes have small recovery loss.

Therefore, the resonant converter has high efficiency when its switching frequency is equal to resonant. From Fig.2-10, output and input voltages are virtually connected together. The resonant converter has also one voltage gain.

2.6.2 Switching Frequency greater than resonant frequency

If the LLC resonant converter operates with the range of switching frequency greater than the resonant frequency, the converter has similar property as the series resonant converter SRC. In forward mode of operation with this range of switching frequency, ZVS on the primary full-bridge switches is occurred due to high turn-off current. But this large turn-off current results for high loss while the secondary intrinsic full-bridge diodes have large di/dt ratio. Due to high di/dt ratio during the turn-off the diodes are under the pressure of voltage stress, which make the converter less reliable for application.

Therefore, the resonant converter has less efficiency when it is compared with the switching frequency which is equal to the resonant. From Fig.2-10, output and input voltages are virtually connected together. The resonant converter has lower than one voltage gain. However, as it shown in the figure the LLC resonant converter can achieve gains larger, equal or less than to one.

2.6.3 Switching Frequency less than resonant frequency

If the LLC resonant converter operates with the range of switching frequency lower than the resonant frequency, the converter has similar property as the parallel resonant converter PRC. Similar to the above two sub-sections the converter is able to achieve gain(Q) smaller, higher or equal to 1.

Chapter 3- Isolated Bi-Directional DC-DC Converter

3.1 Introduction

This chapter present detail description on the selected bi-directional DC-DC converter described in chapter-2 for telecommunication application. At the beginning the topology evaluation for full-bridge current-fed and voltage-fed are the selected topologies[34]. Then the working principle of the converter will be discussed in both cases; discharging and charging mode of operation will be discussed. Each mode of operation will be followed by simulation result and all the simulation results are obtained by LTspice, Power Electronic Simulator(PSIM) and Mat-lab Simulink.

3.2 Topology of Bi-directional DC-DC LLC resonant converter

As mentioned in the introduction(i.e. chapter one) different types of bi-directional dc-dc converter types are categorized. Non-isolated Buck-boost, and isolated dual active full-bridge are typically known topologies in bidirectional dc-dc converters. Dual active full-bridge isolated bi-directional dc-dc converter is the proper selection for this paper with LLC resonant converter. Isolated dual active full-bridge type of bi-directional topology has the following advantages over non-isolated buck-boost bidirectional dc-dc converters:

- Electrical isolation between input and output is guaranteed; system protection is possible when output load short circuit takes place
- Higher step-up ratio can be implemented due to the transformer turn ratio which is impossible in practical for duty ratio
- The transformer can be served as storage energy and balancing the impedance variations between two side etc.

For these reasonable and other advantages isolated full-bridge topology is preferable to select for bi-directional dc-dc LLC resonant converter. The dual active full-bridge isolated bi-direction dc-dc LLC resonant converter topology is sketched in Fig.3-1. Full-bridge topology of isolated bi-directional dc-dc LLC converter contains two active switch bridge on both sides of the transformer. The active switch bridge on the high voltage side is fed by utility while the low side

voltage is fed by current source for charging mode of operation and reverse for dischargi
of operation.

The LLC resonant converter is placed on both sides of the full-bridge. The LLC resonan
topology has high quality to reduce losses due to circulating energy within the converter
leads for balancing the impedance on both sides of the isolations and prevents net flow o
from any side of the isolation[35]. Therefore the LLC resonant converter prevents losse
energy circulation both in the transformer and full-bridge switch.

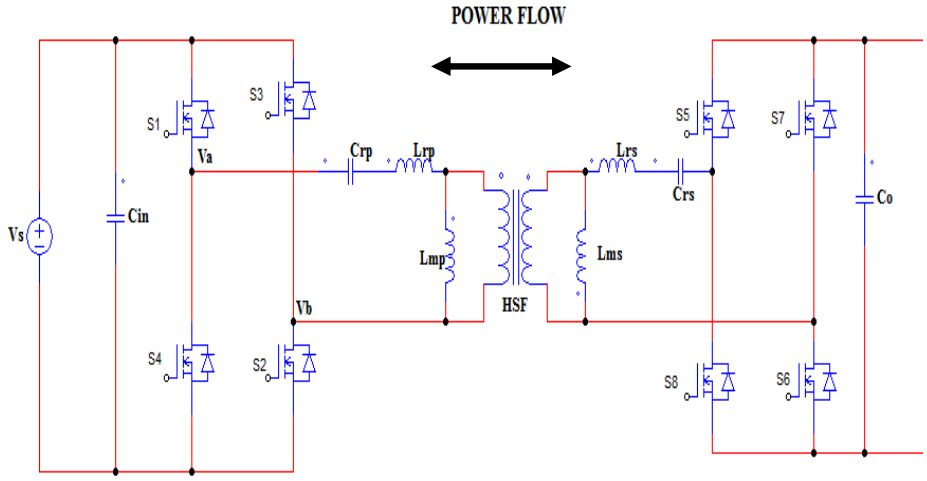

Fig.3- 1: High voltage side with voltage-fed converter and with low side current-fed

From Fig.3-1 due to low voltage, high current and high switching frequency as a re
primary and secondary side full-bridge switches are selected as MOSFET's. Since the sv
frequency of the converter is ranged from 100KHz to 150KHz, it is suitable to select MO
for this dc-dc converter rather than IGBT's which are applicable for high voltage
switching frequency. The full-wave bridge inverter and rectifier contains eight M
switches in total for dual active full-bridge.

Implementing power MOSFET's in bi-directional dc-dc converter in the inverting
converter zero voltage switching is required. Since the converter has MOSFETs it ne

current switching by adding series inductor-resistor component to the output in order to b current flow through the intrinsic diode of the MOSFET's[38].

High and medium power bi-directional dc-dc resonant converters contain both LLC reso transformer isolation and these use to minimize overshoot voltage during switching ti from on-state to off-state. These have also the ability of zero voltage switching due to stored in resonant and transformer leakage inductances[36].

3.3 Operation of the converter and simulation results

The isolated bidirectional LLC resonant converter has two modes of operation shown in In the charging mode power flow from the dc-bus utility to battery or load but in the disc mode of operation power flow from the battery to the dc-bus when power interruption the source.

3.3.1 Charging mode of operation

In LLC resonant bidirectional dc-dc converter at the step down mode of operation power shown in Fig.3-2. The 400V voltage source step-down to 48V output either to load or depending on the application of the converter. In this mode of operation the resonant con implements zero voltage switching and zero current switching application[37].

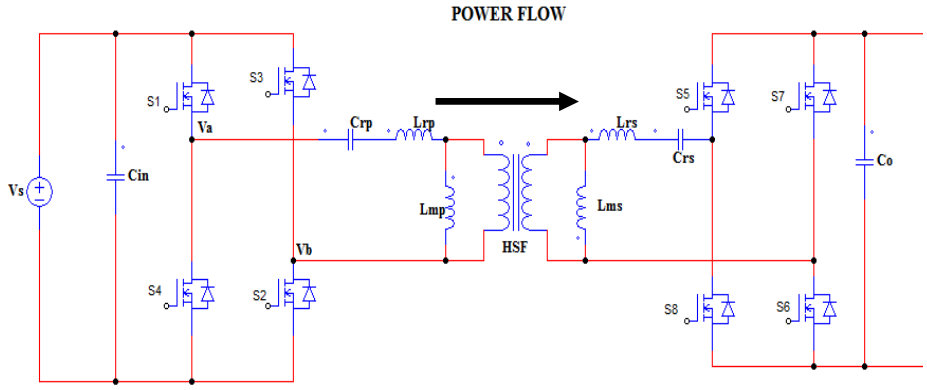

Fig.3- 2: Bidirectional DC-DC converter in step-down mode of operation

In this mode energy flow from the DC-source to battery or load of the application. Switches S_1, S_2, S_3 and S_4 gate signal from the controller while intrinsic diodes in S_5, S_6, S_7 and S_8 serves as rectification of the sinusoidal source to the load and Fig.3-2 and Fig.3-3 indicates the operation of charging mode. The dc source supplies power to dual active bridge converter and then to the battery or load. The input voltage is step down by the transformer and either the battery is charged or the load gates a nominal voltage V_{out}. The MOSFET S_1, S_2, S_3 and S_4 on the primary full-bridge side have gate signals with less than 0.5 duty cycle due to dead time added to the controller, while diodes of S_5, S_6, S_7 and S_8 give rectification purpose for this mode of operation. This dead time is important to overcome the short circuit that occur during over lapping of time rise and time fail of the MOSFET's.

The operation of the converter is in every period of *Ts* and it has four stages operation for each switching time with the following time intervals; T_0-T_1, T_1-T_2, T_2-T_3, and T_3-T_4 intervals as shown in Fig.3-3.

Interval T_0-T_1:

From Fig.3-3 either S_1, and S_2 or S_3 and S_4 are switching alternatively. For this duration of time both S_1, and S_2 switches-off while S_3 and S_4 are turn-on . At time T_0 S_3 and S_4 are gating rise while S_1, and S_2 failed from on-state due to the dead time interval. In this interval the switches either rising or fail due to delay and rise or fail time of the MOSFET's. The primary side of full-bridge output voltage; V_a fails from dc-bus voltage to zero and V_b rise from zero to dc-bus voltage. Since the transformer is not inverted the intrinsic diodes in the MOSFET's in S_5, S_6, gates off-state while the S_7 and S_8 are on-state. The currents in the primary LLC-resonant bank gates fail to its negative bus-current. The output filter component is only capacitor which filters the rectified signal to the battery or load. The energy stored from the previous interval in the resonant and magnetizing inductors provides the load or battery power.

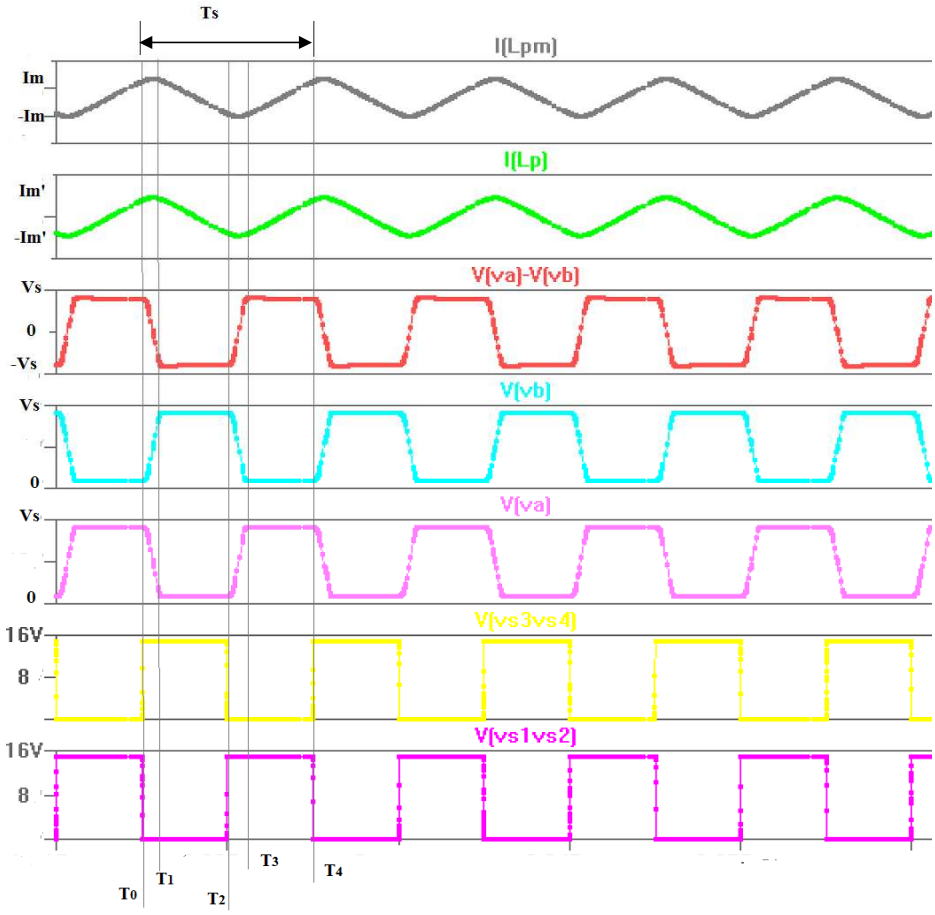

Fig.3- 3:Wave forms for the charging mode of operation

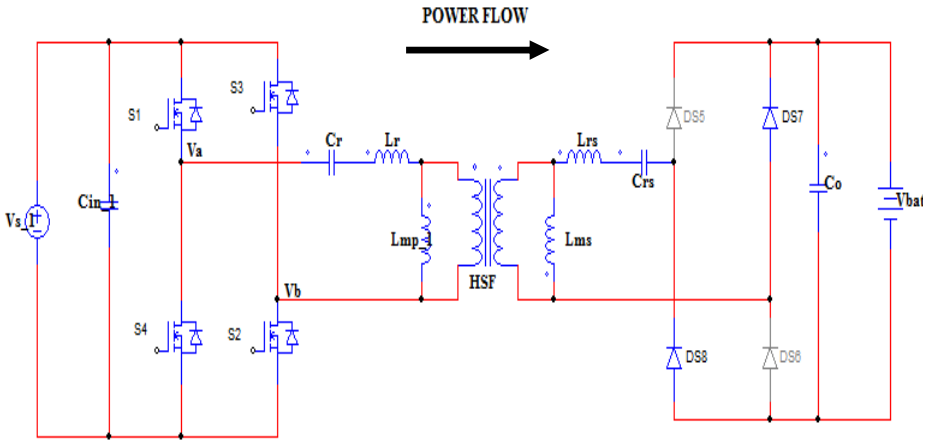

Fig.3- 4: Converter operating in the forward mode in the interval T1-T2

Interval T_1-T_2:

Fig.3-5 shows that the circuit operation of the converter with this time interval. Switch S are turned-on at the instant of T_1 and switches S_1, and S_2 turn-off, while the secon switches remain turn-off. Similar to the first time interval the energy stored in the i supplies power to the load or battery. The primary side of full-bridge output voltage; V_a but V_b is equal to dc-bus voltage. Since the transformer is not inverted the intrinsic diod MOSFET's in S_5, S_6, gates off-state while the S_7 and S_8 on-state. Since the voltage ac inductor is reverse, the inductor current decrease. These provides the intrinsic diodes i full-bridge switches Ds_5 and Ds_6 are reverse biased since the primary side switches S_1 ar not conducting while Ds_7 and Ds_8 are forward biased. The diodes gate product of turn ra magnetizing current (I_{Lmp}*n) from primary side , there by provide rectified current to the

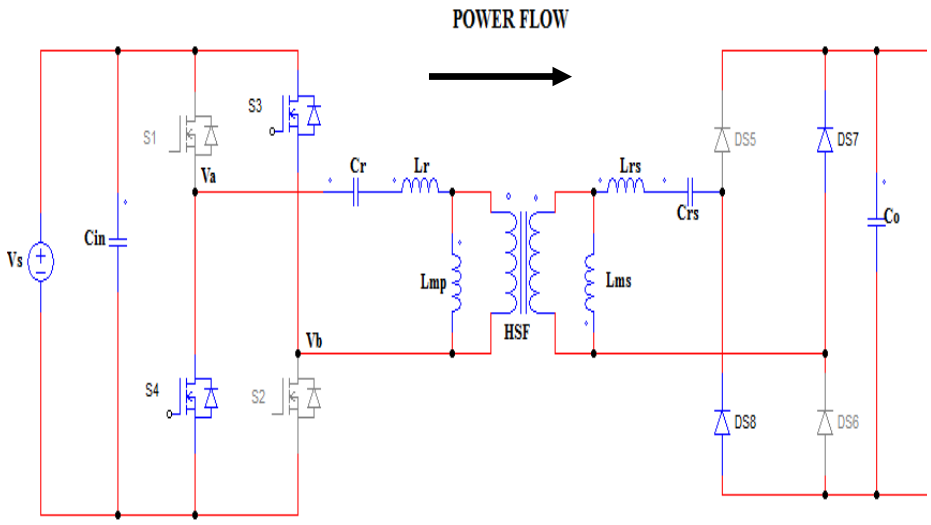

Fig.3- 5: Converter operating in the forward mode in the interval T1-T2

Interval T_2-T_3:

Fig.3-6 describes the converter signal diagram during this time interval. The operatio resonant converter is similar to the time interval T_0-T_1 where S_1 and S_2 rise switches-o S_3 and S_4 are go-down until T_3. The switches are linearly rise or fall due to the intrins conductor structural property of the switches. Therefore the switches in nature never cha state directly from on-state to off-state or alternatively. Since the switches have time rise they change the state linearly.

The primary side of full-bridge output voltage; V_a rise from zero voltage value to voltage but V_b go-down from dc-bus voltage to zero. Since the transformer is not inve intrinsic diodes in the MOSFET's in S_5, S_6, gates on-state while intrinsic diodes in S_7 an off-state.

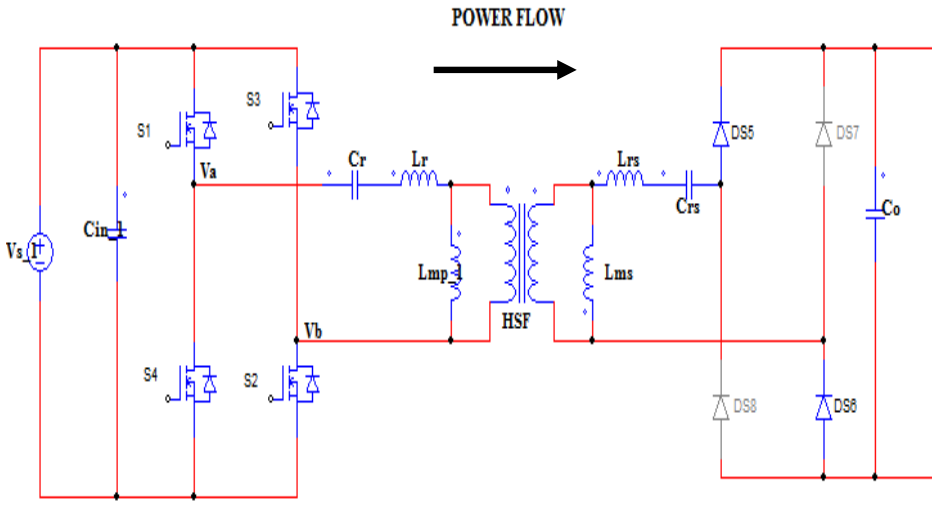

Fig.3- 6: Converter operating in the forward mode in the interval T2-T3

Interval T_3-T_4:

The converter operation in this case is similar to the time interval T_1-T_2. The first half-b the primary sides(i.e. S_1 and S_2) are turn-on, while the S_3 and S_4 switches are turn-off. shows the circuit operation of the converter with this time interval. Switch S_1 and S_2 are on at the instant of T_3 and switches S_3, and S_4 are turn-off, while the second bridge remain turn-off.

Reverse to the T_1-T_2 time interval energy is storing in the inductors from the supplies pc voltage supply. The primary side of full-bridge output voltage; V_b is zero but V_a is equ bus voltage. Since the transformer is not inverted the intrinsic diodes in the MOSFET's i turns to off-state while the S_6 and S_5 turn-on. Since the voltage across the inductor is for inductor current increase and provides the intrinsic diodes in the second full-bridge swit and Ds_8 are forward biased whereas the primary side switches S_3 and S_4 are switched-c Ds_5 and Ds_6 are Reverse biased. The diodes gate product of turn ratio and magnetizing (I_{Lmp}*n) from primary side , there by provide rectified current to the load.

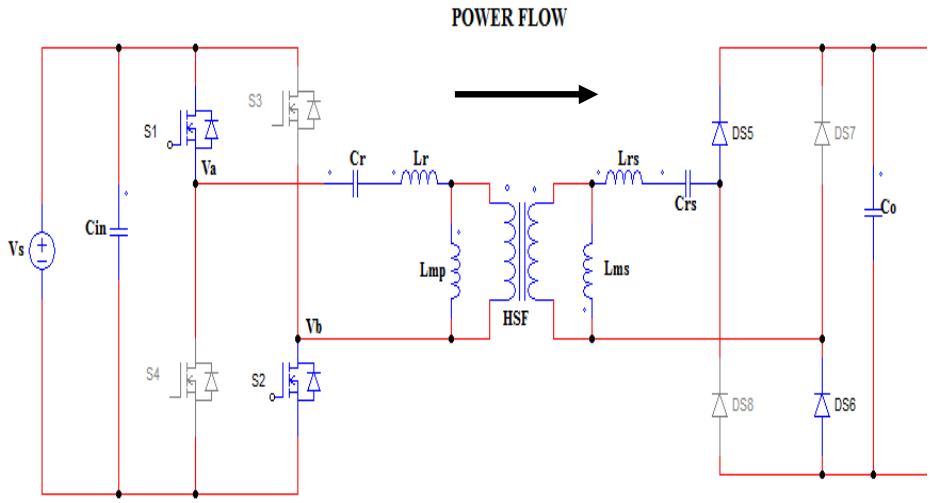

Fig.3- 7: Converter operating in the forward mode in the interval T3-T4

Voltage and current output:

The proposed isolated bi-directional DC-DC converter validates proposed high efficienc flow. Fig.3-8 indicates the simulation result of the converter with selected values parameter from the given specification, selected materials and selection of the paramete resonant component from previous chapter LLC resonant.

Fig.3.8 shows that the DC-DC converter has high efficiency with small ripple of the V_b The ripple value of output voltage and current is less than 1% and its Efficiency is arou Which is high achievement in decreasing the ripple as well as excellent efficiency for e the life time of the converter components specially for MOSFETs.

As mentioned in the earlier chapter, zero voltage switching and zero current switcl benefits of LLC resonant in the converter. Therefore the converter will be redu conduction loss during the freewheeling cycle during the high voltage-side of the fu switch due to zero voltage switching application.

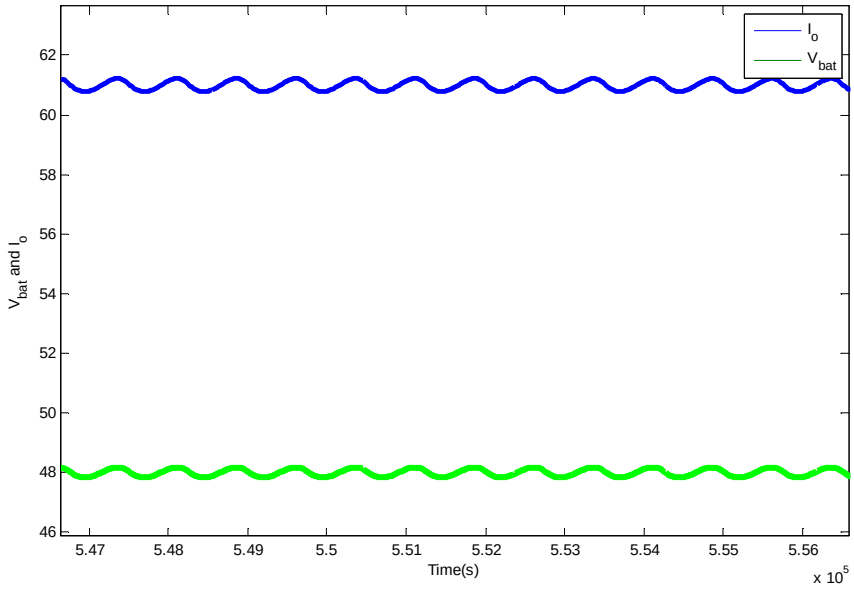

Fig.3- 8: Voltage and current output in charging mode

3.3.2 Forward mode of operation with flux imbalance

The four time intervals described are considered as ideal without considering flux imbalance. Therefore the dual active full-bridge bi-directional converter in the forward mode of operation is considered with balanced flux between the two sides of the transformer. First it need to define the flux balance and saturation of transformer. If the average output voltage applied to the primary side of the transformer where the positive pulse is not the same as the negative pulse for each cycle the transformer flux balance can't be occurred. Therefore the transformer flux density increase with the number of cycle and finally flux density saturation occurred. Gradually the saturation of the transformer goes to the slope of hysteresis curve. The magnetizing inductance of the transformer increases with the proportion of hysteresis curve and finally gates saturation and burns down the switching MOSFET's and gate drive controlling components.

The node voltages at the junction A and B each contains half cycle DC-bus voltages may not be the same. This condition of the full-bridge output voltage may result in saturation of the

transformer core metal and sever the switching MOSFET's . Fig.3-1 shows that the tank serves for balancing the voltage difference between each half cycle output voltage .

3.4 Backup/Current Fed Mode

The converter operates in discharging mode of operation when dc-bus supply p interrupted. In the lack of dc-bus power supply the battery start discharge in order to su the rest of power network. Fig.3-9 shows the step-up from 48V to 400V where the batte source of the power. The secondary full-bridge switches S_5, S_6, S_7 and S_8 are active pa for this mode of operation and the first full-bridge switches S_1, S_2, S_3 and S_4 are always but their intrinsic diodes are participate in rectification.

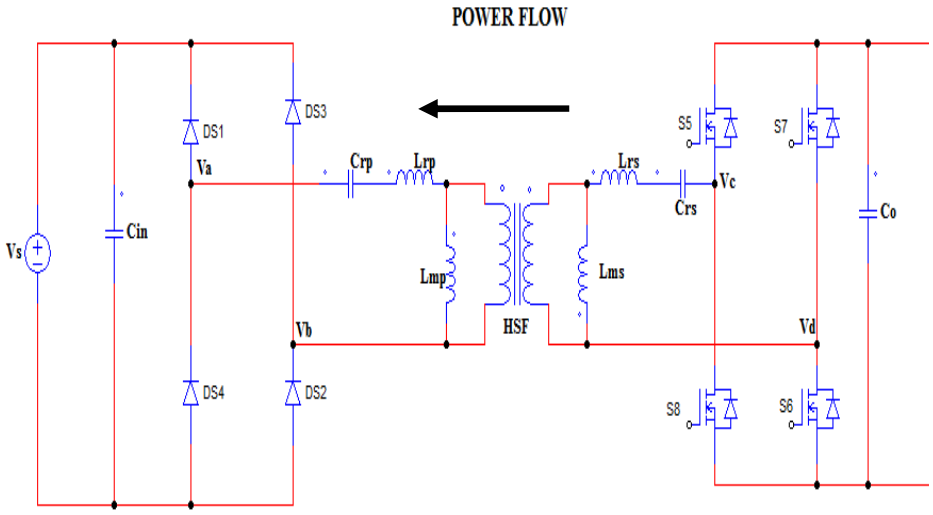

Fig.3- 9: Bidirectional DC-DC converter in step-up mode of operation

The duty ratio of the bidirectional is not exactly 0.5 due to the switch intrinsic co property. Therefore from the graphic characteristic of the MOSFET's they have appro 0.45 duty ratio due to smoothly rise and fall of the MOSFET's. Rectification at the carried out by intrinsic MOSFET diode's of S_1, S_2, S_3 and S_4 switches. The step-up described with the wave-form shown in Fig.3-10. As described in the step-down or mode of operation the resonant and magnetizing currents are assumed continuous. T form describes in the time interval between T_0 and T_4 for the converter operation within a

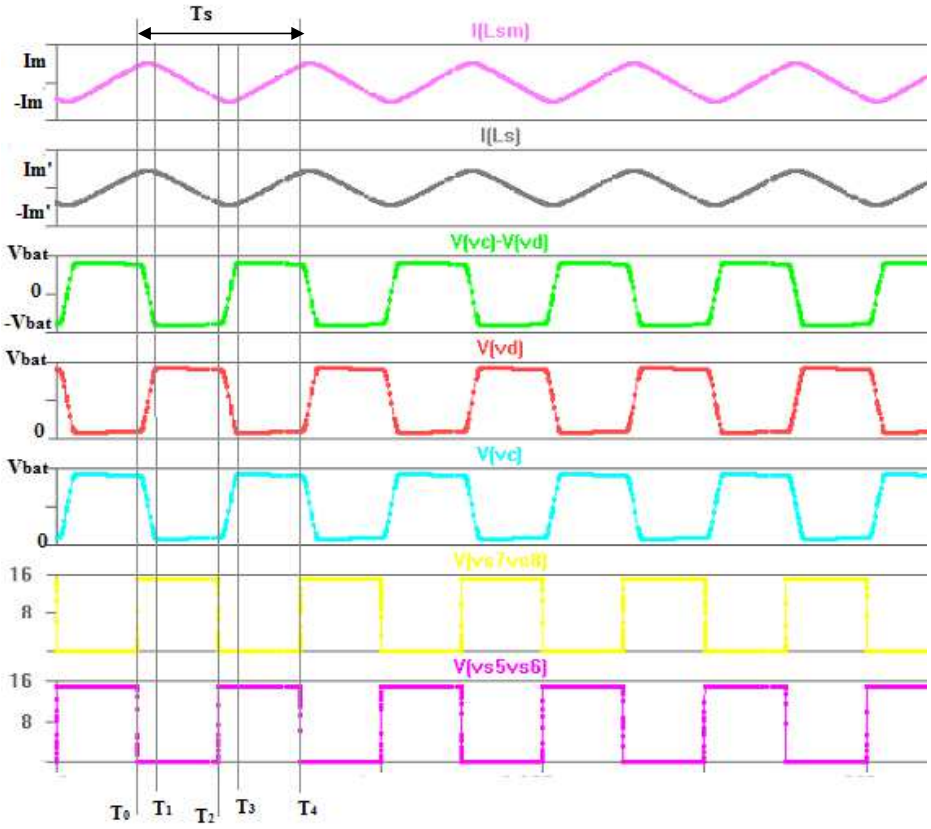

Fig.3- 10: Wave forms for the discharging mode of operation

Interval T_0 - T_1:

Switches S_5 and S_6 are on the turn-on state before the time instance of T_0 and then after begun to fall-down until T_1 ; while switches S_7 and S_8 on the off-state before the time ins T_0. The converter circuit diagram at this time interval is difficult to identify due to its property of the MOSFET's all have transition period either from on state to off-state versa. The secondary transformer winding subject to magnetizing inductor, which store that appear across the battery. From Fig.3-10 the inductor currents increase with second parabolic graph which shares equally by S_7 and S_8 switches. During this time interval th is stored in the C_{in} and provide the load power through the dc-bus system.

The energy is transferred to the dc-bus from the battery by S_7 and S_8 switches intrinsi rectification. The DS_7 and DS_8 intrinsic diodes are conducting while DS_5 and DS_6 are reverse biased.

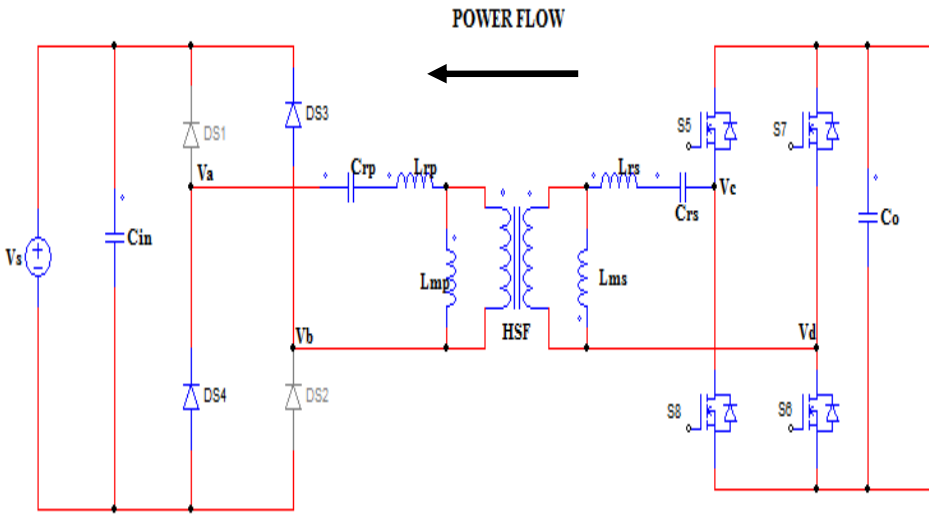

Fig.3- 11: Converter operating in the reverse mode for T3-T4 interval

Interval T_1 - T_2:

S_7 and S_8 at instant T_1 continue to remain on-state while S_5 and S_6 are turned-off du interval of time which is clearly described in Fig.3-12. From the waveform shown in Fig. energy stored in the Inductors during the two previous intervals then provides load pow dc-bus by rectification through the intrinsic MOSFET's diode of the primary full-bric Since the power flow to the dc-bus, the inductor linearly decrease until T_2 time interval.

In this time interval V_c is zero but V_d is equal to dc-battery voltage. Since the transform inverted the intrinsic diodes in the MOSFET's in S_1, and S_2, gates off-state while the DS_4 intrinsic diodes are turned on. Thus, they have the same current flow through the diodes of the S_3 and S_4 switches.

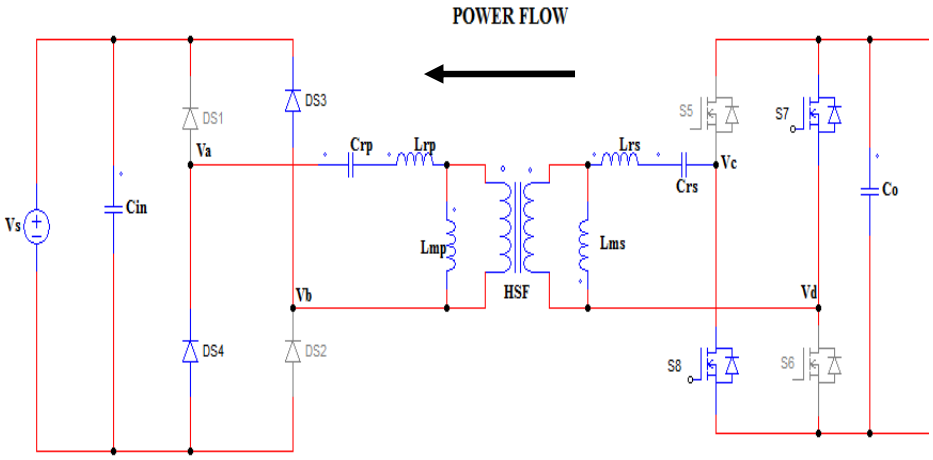

Fig.3- 12: Converter operating in the reverse mode for T3-T4 interval

Interval T_2 - T_3:

Fig.3-10 shows that interval ***T_2 - T_3*** have similarity with T_0 - T_1 interval. S_5 and S_6 switc signal from gate drive and turn from off-state to on-state, while S_7 and S_8 switches turn on-state to off-state due to the intrinsic property of MOSFET's. Since S_5 and S_6 are going on the inductors core store energy with second order rise of current, which is not the san above interval with linear rise of current. Voltage across node C rises linearly from zero V_{bat} at T_3, similarly V_d decreases linearly from V_{bat} to zero with corresponding time.

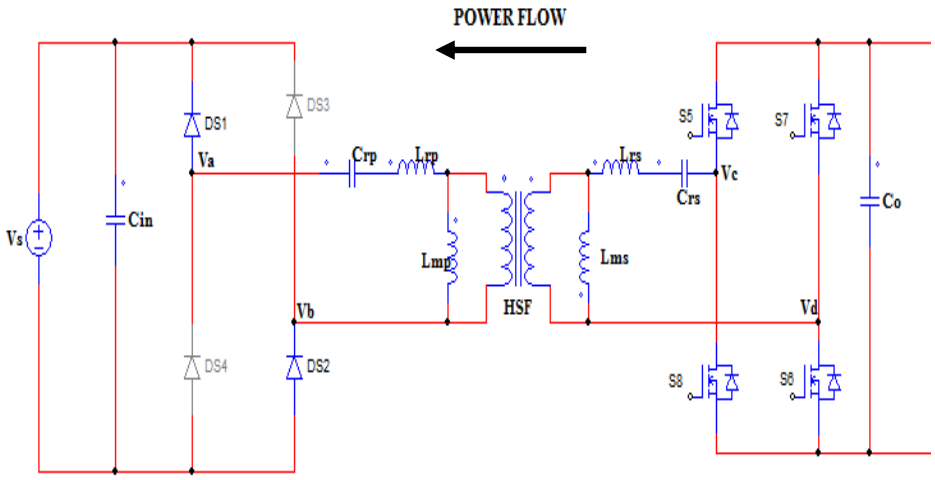

Fig.3- 13: Converter operating in the reverse mode for T3-T4 interval

Interval T_3 - T_4:

The converter circuit operating during this time interval is shown in Fig.3-14. The wave
the signal is similar to T_1- T_2 time interval. As shown in the wave form for this time int
inductors store energy due to conducting of S_5 and S_6.

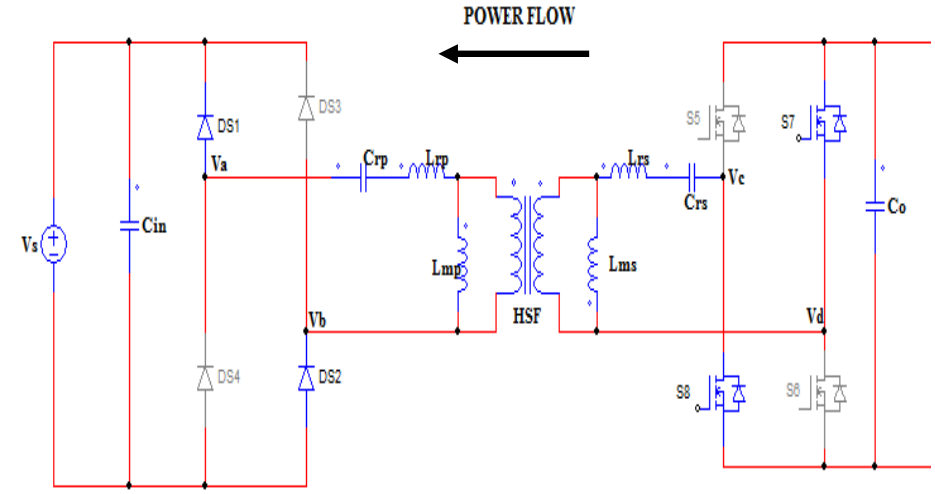

Fig.3- 14: Converter operating in the reverse mode for T3-T4 interval

Voltage and current output:

In the forward mode of operation the output voltage and current detailed discussed. Here the difference is the change of power from battery to the DC-bus source. The proposed isolated bi-directional DC-DC converter validates proposed high efficiency power flow. Fig.3-15 indicates that the simulation result of the converter with selected values of the parameter from the given specification, selected materials and selection of the parameters of the resonant component from previous chapter LLC resonant tank.

Fig.3.15 shows that similar to forward mode of operation the converter has high efficiency with small ripple of the V_s and I_s. The ripple value of output voltage and current is less than 1% and its efficiency is around 97%. This is great achievement in decreasing the voltage and current ripple therefore this prototype is better choice for extending the life time of the converter components specially for MOSFETs.

The benefits of LLC resonant in the converter as mentioned in the earlier chapter is zero voltage switching and current switching. Therefore the converter will be reduced the conduction loss during the freewheeling cycle during the high voltage-side of the full-bridge switch due to zero voltage switching application.

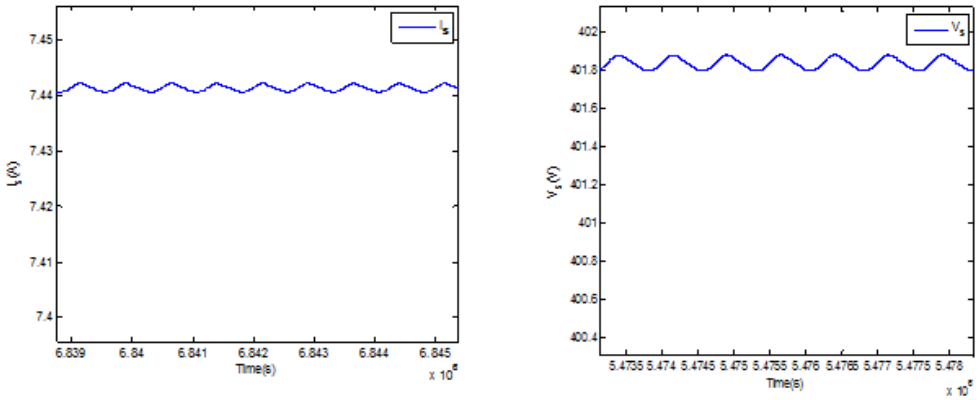

Fig.3- 15: Voltage and current during discharging mode of operation

Chapter 4- Small Signal Analysis

4.1 Introduction

The converter circuit parameters and their rating values are analyzed at steady state in chapters two LLC resonant topology. The output voltage of the resonant converter is controlled as the output load and input voltage vary by regulating the switching frequency value in DSP-controller to drive the MOSFETs in new frequency. Therefore the dynamic change of output voltage of the converter can be accomplished by applying feedback control from output to the error compensator as shown in Fig.4-1[39].

The compensated error amplifier compares' the reference value with the feedback or current value in order to modify switching frequency of gate drives in the resonant converter. In order to design the compensator; developing mathematical expression of the converter plant at dynamic performance is the basic tool for developing the controller of the converter. Therefore the dynamic performance of the resonant converter plant can be expressed in small signal transfer function using; harmonic function, extended describing function and steady state expressions. These transfer function of the plant uses to design the compensate error amplifier(controller); which gives to control overall system based on dynamic response of the system.

The isolated bi-directional dc-dc LLC resonant converter system shown in Fig. 4-1 contains two transfer functions; $G_p(s)$ is the Laplace-Domain transfer function of the plant that is the resonant converter and $G_c(s)$ is the controller transfer function which control the output voltage by varying the switching frequency.

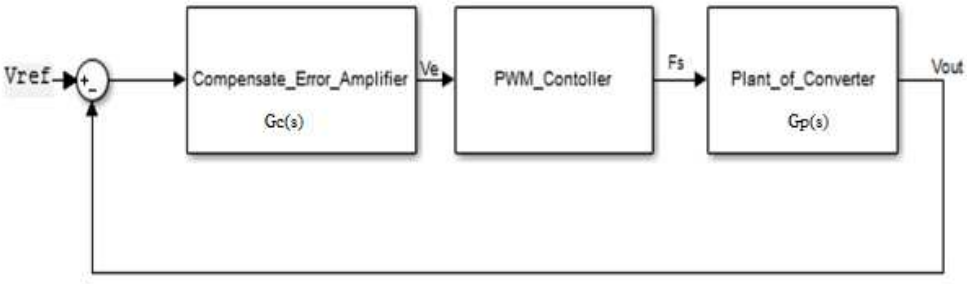

Fig.4- 1: The block diagram of the system including feedback.

This chapter describes the small signal analysis for both forward and backward mode of operation. The transfer function of the system is developed under voltage control mode which also used to analyze and design of the compensator under the closed control loop.

4.2 State Space Approach

In nature power supply from switching devices are not linear; so that they are discontinuous which needs techniques in order to linear the system and the circuit can be analyzed. State space modeling is the best way to tackle the non-linear system[40-41] by approximating the non-linear operating points to linear mathematical expression.

State space modeling is mathematical expression of non-linear operating points in linear expression by considering some approximations or assumptions. The state space averaging approach described in [40-42] are use to derive the open loop and control loop transfer function. There are some assumption for driving the transfer function in the next sub-topic.

4.3 Considered Assumptions for Simplifying Small Signal Model

The assumptions for simplifying the performance of the resonant converter in small signal modeling with the following procedures.

- ✓ The output ripple is negligible.
- ✓ The switching devices are instantaneous switching from state to state using the first harmonic method.
- ✓ The output filter frequency is around two times the switching frequency

4.4 Small signal analysis for charging mode of operation

In forward mode the small signal analysis starts by transferring secondary circuit parameters to the primary side by using turn ratio of transformer. The transfer operations are secondary resonant inductor, resonant capacitor, magnetizing resonant inductor and load. In general there are four steps to analyze the forward small signal[42], which are described as follow:

1) State the time variant non-linear state equations

2) Harmonic approximation

3) Applying extended describing function

4) Developing the states space Model

4.4.1 State the time variant non-linear state equations

As described in the considering assumption to analysis small signal is simplifying the construction of the converter by using ideal switching device. To have simplified topology of the converter, then transferring the resonant tank from secondary to primary side will give non-complex approach for state equations analysis. The equivalent circuit for the resonant converter is built as the following three figures with the V_{ab} square wave signal output of the first full-bridge converter.

The simulation of the small signal is sampled for the first harmonic components because the assumption for simplifying the analysis of the small signal. Here are the steps to gate the final equivalent circuit signal design of resonant converter.

Equivalent circuit LLC Resonant Converter

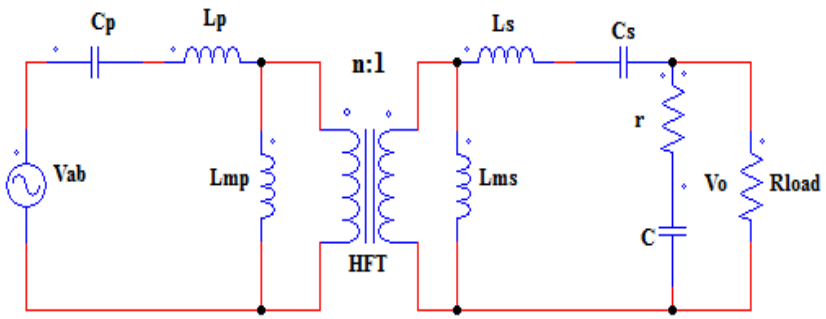

Fig.4- 2: Equivalent circuit with two resonant tank

V_{ab} AC-voltage with first harmonic peak value of the output from the primary full-bridge converter

s(secondary), p(primary), mp(primary magnetizing component) and ms(secondary magnetizing component)

Transferring the secondary components of LLC resonant tank parameters to primary side of the transformer by using transformer turn ratio($n = \frac{Np}{Ns}$)

$$Ls' = Ls * n^2 \qquad Cs' = Cs * n^2 \qquad Lms' = Lms * n^2$$

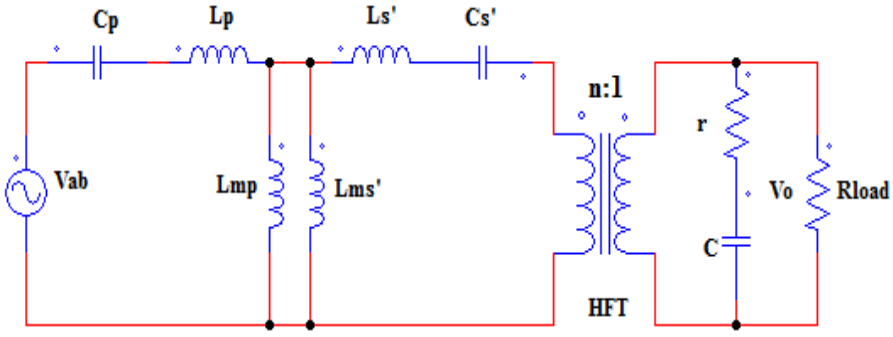

Fig.4- 3: Equivalent circuit with transferred resonant to primary side

Furthermore simplify the converter resonant tank by assembling the two parallel mag components:

Lm = Lms//Lms'

The equivalent circuit of LLC resonant converter shown in Fig.4-3 is the simplifie diagram from Fig.4-2 by combining the parallel magnetizing inductors into one inductor.

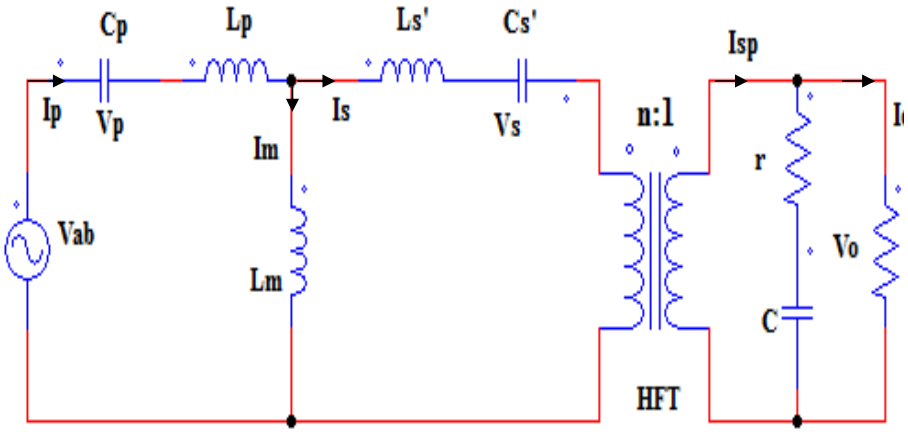

Fig.4- 4: Equivalent circuit with equivalent resonant banks on the primary side of the convert

From the equivalent circuit in Fig.4-3 input voltage to the resonant tank can be analyzed

$$v_{ab} = v_p + v_m + l_p \frac{di_p}{dt} \quad \text{or}$$

$$v_{ab} = v_p + v_s + l_p \frac{di_p}{dt} + sgn(i_s) * v_c' \quad (1)$$

Where $sgn(i_s) = \{-1, if\ v_c' < 0$ discharging mode of operation

$= \{1, if\ v_c' > 0$ charging mode of operation

$$v_m = l_m \frac{di_m}{dt} = l_m \frac{di_p}{dt} - l_m \frac{di_s}{dt} \quad (2)$$

Substituting equation 2 into 1:

$$v_{ab} = v_p - l_m \frac{di_s}{dt} + (l_p + l_m) \frac{di_p}{dt} \qquad (3)$$

Similar to the input voltage of resonant tank is possible to develop the output voltage at the secondary side of the transformer using Kirchhoff's law:

$$v_o = \frac{r * R_l}{r + R_l} abs(I_{sp}) + \frac{R_l}{r + R_l} v_c \qquad (4)$$

4.4.2 Appling harmonic approximation

On this thesis the converter is designed based on desired and controlled output voltage due to the variation of load. As discussed and shown in chapter 2 the resonant converter has very low switching voltage loss and zero current switching that is why LLC resonant converter substitutes for pulse width modulation [44]. Therefore, this is the best approach of minimizing loss by applying frequency control variable in order to have constant output voltage . This can be achieved using Fourier series expansion form.

Using the Fourier series expansion form which decomposes periodic function or periodic signals in to a sum simplified oscillating functions(as sine and cosine) components[42-43]. The general Fourier series expansion form is given as the following equation for the first harmonic and general component derivation.

$$f(x) = ao \pm \sum_{n=1}^{\infty} (a_n \sin nx \pm b_n \cos nx) \quad (5)$$

Considering only the first component of the harmonic values; since the fist harmonic is enough to manipulate for the simulation. Whereas the analysis is complex when the analysis consider above two harmonic components for the development of mathematical expression of the resonant converter plant. Therefore the mathematical expression for first harmonic component of a function as:

$$f(x) = \mathrm{a}_1 \sin x \pm b_1 \cos x \qquad (6)$$

From the above general expression of first harmonic component approximation $i_p(t)$, $i_s(t)$, $v_p(t)$ and $v_s(t)$ can be expressed and decomposed into sine and cosine component as following mathematical representation:

$$i_p(t) = \mathrm{i_{ps}}\sin\omega t - i_{pc}\cos\omega t \qquad (7)$$

$$i_s(t) = \mathrm{i_{ss}}\sin\omega t - i_{sc}\cos\omega t \qquad (8)$$

$$v_s(t) = \mathrm{v_{ss}}\sin\omega t - v_{sc}\cos\omega t \qquad (9)$$

$$v_p(t) = \mathrm{v_{ps}}\sin\omega t - v_{pc}\cos\omega t \qquad (10)$$

The parameters written in small letter indicates they are function of time. From the equivalent circuit diagram shown Fig.4-3, the state equations are defined and decompose into sine and cosine components using Fourier series transformation. The state equations are decomposed in two sine and cosine components as expressed from eq. (14) to (17).

$$v_m = v_s + i_s * R_e + l_s' \frac{di_s}{dt} \qquad (11)$$

$$i_s = c_s' \frac{dv_s}{dt} \qquad (12)$$

$$i_p = c_p \frac{dv_p}{dt} \qquad (13)$$

$$\frac{di_p}{dt} = \frac{di_{ps}}{dt} + \omega i_{pc} - \left(\frac{di_{pc}}{dt} - \omega i_{ps}\right) \qquad (14)$$

$$\frac{di_s}{dt} = \frac{di_{ss}}{dt} + \omega i_{sc} - \left(\frac{di_{sc}}{dt} - \omega i_{ss}\right) \qquad (15)$$

$$\frac{dv_s}{dt} = \frac{dv_{ss}}{dt} + \omega v_{sc} - \left(\frac{dv_{sc}}{dt} - \omega v_{ss}\right) \qquad (16)$$

$$\frac{dv_p}{dt} = \frac{dv_{ps}}{dt} + \omega v_{pc} - \left(\frac{dv_{pc}}{dt} - \omega v_{ps}\right) \qquad (17)$$

R_e is the load transferred from secondary to primary side of the transformer, **s** stands to sine and **c** also stands for cosine components of the functions.

4.4.3 Applying extended describing function

Extended describing function is the mathematical expression of functions for easily understand, analyze, modifying and designing of non-linear systems, since most electrical systems are non-linear systems and complex[45-46]. From the two non-linear equations above equation (1) and (4) can be linear using extended describing function.

$$v_{ab}(t) = f_1(d, v_{in}) \sin \omega_s t - f_5(d, v_{in}) \cos \omega_s t \quad (18)$$

$$sgn(i_{sp}) v_c' = f_2(i_{ss}, i_{sp}, v_c') \sin \omega_s t - f_3(i_{sc}, i_{sp}, v_c') \cos \omega_s t \quad (19)$$

$$i_{sp} = f_4(i_{sc}, i_{ss}) \quad (20)$$

The functions $f_1(d, v_{in}), f_2(i_{ss}, i_{sp}, v_c'), f_3(i_{sc}, i_{sp}, v_c'), f_4(i_{sc}, i_{ss})$ *and* $f_5(d, v_{in})$ are called Extended Describing Function (EDF); also i_{sc} *and* i_{ss} are sine and cosine component of current at the primary side of the transformer.

V_{ab} is the output voltage from the full-bridge converter from the high side of the converter which is shown in the Fig.4-4. Full-bridge output voltage fundamental value can be analyzed using Fourier series expansion clearly described in the following mathematical expressions.

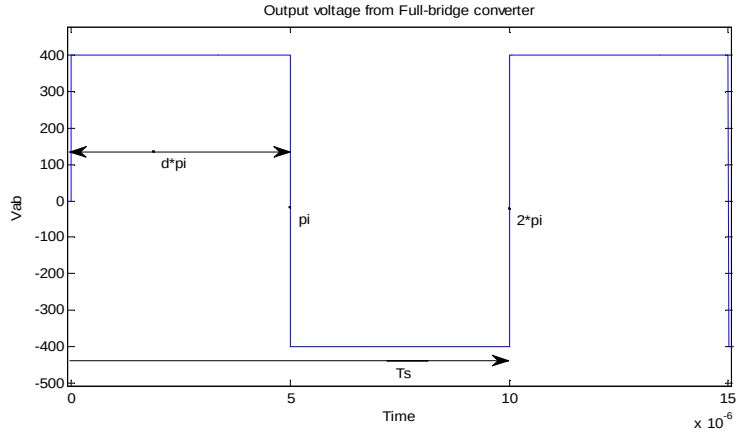

Fig.4- 5: Switch form of full-bridge inverter

$$v_{ab}(t) = f_1(d, v_{in}) \sin \omega_s t$$

$f_1(d, v_{in})$ is amplitude or maximum value of the sine component of the first harmonic. Therefore we can derive from the average value. Where α is phase shift:

$$f_1(d, v_{in}) = \frac{2}{2\pi} \left(\int_{\alpha}^{\pi-\alpha} v_{in} * \sin \omega t \, d\omega t + \int_{\pi+\alpha}^{2\pi-\alpha} v_{in} * \sin \omega t \, d\omega t \right)$$

$$= -\frac{2}{2\pi} v_{in}(\cos \omega t|_{\alpha}^{\pi-\alpha} + \cos \omega t|_{\pi+\alpha}^{2\pi-\alpha})$$

$$= \frac{4}{\pi} v_{in} \cos \alpha \ ,$$

Where α can be related with the duty ratio in general form; even though it is not declared on Fig.4-4.

$$2\alpha = \pi - d * 2\pi \qquad \alpha = \frac{\pi}{2} - d\pi$$

But for this paper since duty cycle is fixed (d = 0.5) which implies $\alpha = 0$. Final we can conclude for our case :

$$f_1(d, v_{in}) = \frac{4}{\pi} v_{in}$$

$$v_{ab}(t) = \frac{4}{\pi} v_{in} \sin \omega_s t \qquad (21)$$

Similar to V_{ab}, secondary voltage can be transferred using extending describing function[42].

$$f_2(i_{ss}, i_{sp}, v_c^{'}) = \frac{4}{\pi} \frac{i_{ss}}{I_s} v_c^{'} \ \ where, v_c^{'} = n v_c$$

$$I_{sp} = n I_s \rightarrow \ I_s = \sqrt{i_{ss}^2 + i_{sc}^2}, \quad therefore$$

$$f_2(i_{ss}, i_{sp}, v_c^{'}) = \frac{4n}{\pi} \frac{i_{ss}}{I_s} v_c = \ v_{sc} \qquad (22) \quad is\ the\ sine\ component$$

Similarly the cosine component is:

$$f_3(i_{sc}, i_{sp}, v_c^{'}) = \frac{4n}{\pi} \frac{i_{sc}}{I_s} v_c = \ v_{cc} \qquad (23)$$

4.4.4 States Space Equation For Forward Mode of Operation

State space is mathematical expression of a physical model as combination of input, output and state variables which is fundamental Fourier series component analyzed from differential equations[47, 48]. But for this case it is selected the first order differential equation due to its simplification and approximate function of the signals. Before developing the state space equation it is better to gate the mathematical expression from time varying functions. So that the

state variable, input and output of different parameters are derived from (1) to (23) time varying equation in addition to Kirchhoff's current and voltage law.

From equation (1) and (2)

$$v_{ab} = v_p + v_m + l_p \frac{di_p}{dt}$$

$$v_{ab} = v_p + l_m \frac{di_p}{dt} - l_m \frac{di_s}{dt} + l_p \frac{di_p}{dt}$$

$$v_{ab} - v_p + l_m \frac{di_s}{dt} = (l_p + l_m) \frac{di_p}{dt}$$

The sine component of i_p current: from eq. 3, 14 and 15

$$v_{abs} - v_{ps} + l_m(\frac{di_{ss}}{dt} + \omega i_{sc}) = (l_p + l_m)(\frac{di_{ps}}{dt} + \omega i_{pc})$$

$$i_{ps} = \frac{1}{l_p + l_m} \int (v_{abs} - v_{ps} + l_m \omega i_{sc}) dt - \int (\omega i_{pc}) dt + \frac{l_m}{l_p + l_m} i_{ss} \qquad (24)$$

the cosine component of i_p current: from eq. (3),(14) and (15)

$$v_{abc} - v_{pc} + l_m(\frac{di_{sc}}{dt} - \omega i_{ss}) = (l_p + l_m)(\frac{di_{pc}}{dt} - \omega i_{ps})$$

$$i_{pc} = \frac{1}{l_p + l_m} \int (v_{abc} - v_{pc} - l_m \omega i_{ss}) dt + \int (\omega i_{ps}) dt + \frac{l_m}{l_p + l_m} i_{sc} \qquad (25)$$

From equation (2) and (3)

$$v_m = l_m \frac{di_m}{dt} = l_m \frac{di_p}{dt} - l_m \frac{di_s}{dt}$$

$$v_m = v_s + i_s * R_e + l_s' \frac{di_s}{dt}$$

$$l_m \frac{di_p}{dt} - v_s - i_s * R_e = (l_s' + l_m) \frac{di_s}{dt}$$

Where Re is equivalent resistance of the secondary side of the transformer transferred to primary side of the transformer.

The sine component i_s current:

$$-i_{ss}R_e - v_{ss} + l_m(\frac{di_{ps}}{dt} + \omega i_{pc}) = (l_s' + l_m)(\frac{di_{ss}}{dt} + \omega i_{sc})$$

$$i_{ss} = \frac{1}{l_s' + l_m}\int(-i_{ss}R_e - v_{ss} + l_m\omega i_{pc})dt - \int(\omega i_{sc})dt + \frac{l_m}{l_s' + l_m}i_{ps} \quad (26)$$

The cosine component of i_s current:

$$-i_{sc}R_e - v_{sc} + l_m(\frac{di_{pc}}{dt} - \omega i_{ps}) = (l_m + l_s')(\frac{di_{sc}}{dt} - \omega i_{ss})$$

$$i_{sc} = \frac{1}{l_m + l_s'}\int(-i_{ss}R_e - v_{ss} + l_m\omega i_{sc} - \omega i_{sc})dt + \frac{l_m}{l_m + l_s'}i_{ps} \quad (27)$$

Sine and cosine component of current on the resonant thank component transferred from the secondary to primary side of the transformer are derived as the following mathematical expressions from equation (12).

$$i_s = c_s'\frac{dv_s}{dt}$$

i_s sine component

$$i_{ss} = c_s'(\frac{dv_{ss}}{dt} + \omega v_{sc})$$

$$v_{ss} = \int(\frac{1}{c_s'}i_{ss} - \omega v_{sc})dt \quad (28)$$

i_s cosine component

$$i_{sc} = c_s'(\frac{dv_{sc}}{dt} - \omega v_{ss})$$

$$v_{sc} = \int (\frac{1}{c_s'} i_{sc} + \omega v_{ss}) dt \qquad (29)$$

From equation (13) sine and cosine component of the voltage at primary side of the resonant capacitor:

$$i_p = c_p \frac{dv_p}{dt}$$

v_p **sine component**

$$i_{ps} = c_s' (\frac{dv_{ps}}{dt} + \omega v_{pc})$$

$$v_{ps} = \int (\frac{1}{c_s'} i_{ps} - \omega v_{pc}) dt \qquad (30)$$

v_p **cosine component**

$$i_{pc} = c_s' (\frac{dv_{pc}}{dt} - \omega v_{ps})$$

$$v_{pc} = \int (\frac{1}{c_s'} i_{pc} - \omega v_{ps}) dt \qquad (31)$$

The output current can be analyzed using Kirchhoff's current law:

$$i_c = I_{sp} - i_o$$

$$i_c = C \frac{dv_c}{dt}$$

Where i_c filter current, I_{sc} peak output current of secondary resonant tank and i_o, is load current with I_o peak value.

$$I_{sp} = \frac{2n}{\pi} \sqrt{{I_{ss}}^2 + {I_{sc}}^2}$$

$$V_c = \frac{1}{c} \int (\frac{2n}{\pi} \sqrt{{I_{ss}}^2 + {I_{sc}}^2} - \frac{V_{out}}{R_l}) dt \qquad (32)$$

$$R_e = \frac{8n^2}{\pi^2} R_l$$

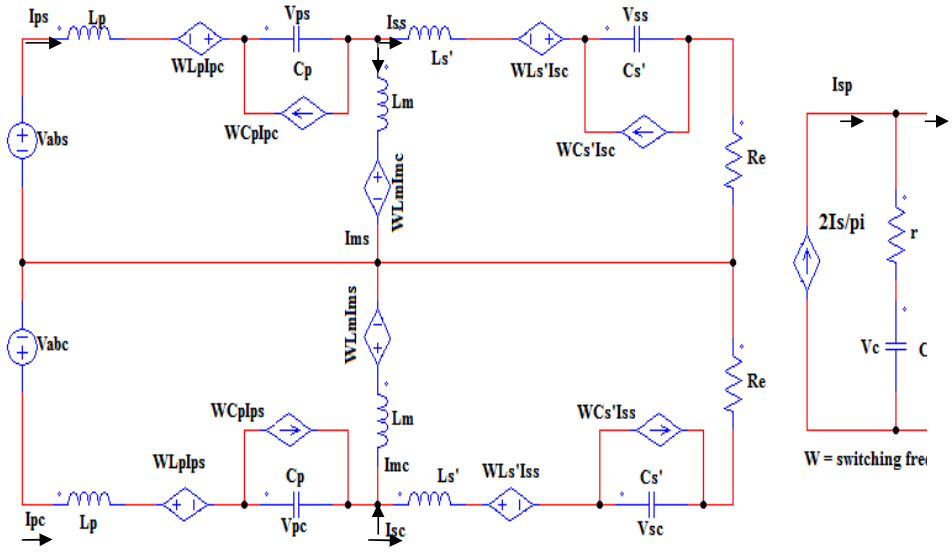

Fig.4- 6: The large signal modeling of sine and cosine components

The state space equations from eq. 24 to 32 also known as time domain approach whi simplified and compact way to model the state space using simulink tool with nine differ equations. Fig.4-5 represents large small signal of the equations derived above from eq Therefore the state space representation of LLC resonant converter can be modeled u general expression of state space model as:

$$\frac{dx'}{dt} = Ax' + Bu' \qquad (33)$$

$$y' = Cx' + Du' \qquad (34)$$

Where $x' = (i_{ps}\ i_{pc}\ i_{ss}\ i_{sc}\ v_{ps}\ v_{pc}\ v_{ss}\ v_{sc}\ v_c)^T$ state variables of the system

$u = (\omega)$ control input which is frequency

From the above equations and the parameter values stated in chapter 2 and their state space coefficient matrix are analyzed using mat lab simulink model from the simulation of the whole converter plant. Therefore the matrix values for state space coefficient is shown in the following matrix form.

$$A = 10^6 * \begin{bmatrix} -0.01 & 0 & 0 & 0.00 & 0.00 & 0 & 0 & 0.04 & 0.05 \\ 0 & 0 & 0 & 4.80 & 3.27 & 0.63 & 0 & 0 & 0 \\ 0 & 0 & 0 & 3.27 & 4.78 & 0 & 0.63 & 0 & 0 \\ 0 & -0.05 & 0 & 0 & 0 & 0 & 0 & 0.63 & 0.00 \\ 0 & 0 & -0.05 & -2.78 & -4.07 & 0 & 0 & 0.00 & 0.63 \\ 0 & -0.63 & 0 & 0 & 0 & 0 & 0 & 4.80 & 3.27 \\ 0 & 0 & -0.63 & 0 & 0 & 0 & 0 & 3.27 & 4.80 \\ 0 & 0 & 0 & -0.63 & 0 & -0.05 & 0 & 0 & 0 \\ 0 & 0 & 0 & -0.00 & -0.63 & 0 & -0.05 & -2.8 & -4.07 \end{bmatrix}$$

$$B = \begin{bmatrix} 0 \\ -235.994 \\ -0.0141 \\ 3.629 \\ 3.6397 \\ -46.651 \\ -46.522 \\ -57.975 \\ 39.652 \end{bmatrix} \quad C = \begin{bmatrix} 0.9987 & 0 & 0 & 0.000 & 0 & 0 & 0 & 0.0068 & 0.0099 \end{bmatrix} \quad D = [0]$$

4.4.5 Comparing simulink results for the step response

The dual active bridge resonant converter is modulated with variable switching frequency depending on the load and fixed duty ratio for this case duty ratio is half. The voltage transient step response of LLC resonant DAB converter under this frequency controlling strategy[49, 50] is analyzed under open loop operation. The converter dynamic model is expressed in state space which control output DC voltage constant when change of load or power flow by controlling switching frequency f_s state variable. From the above developed dynamic model in simulink

which defines the resonant converter in terms of the switching functions in the Fouri harmonic equivalent states. Fig.4-6,7 and 8 shows step response when load cha disturbance occurred on the load for forward mode of operation. As shown in Fig.4-6 t change of switching frequency from 100 to 101KHz, this leads to decrease the output Since it is assumed an open loop system the converter output voltage will have less desired voltage. In this case the step responses are not simulate with feedback contro shows the step response with change frequency.

The simulation takes place at three different conditions; dynamic non-linear step r dynamic linear step response and full-bridge step response or the real time simulatic though all have similar step response, but the step response in the full-bridge has mo than the dynamic linear and non-linear response. The simulation difference between lin linear shown in Fig.4-6,7and8 with a step-frequency from 100KHz to 101KHz. From Fig simulation results shows full-bridge converter has high magnitude harmonic value du step change of the frequency but the two step response haven't ripple values. For all sim the frequency step change takes after 0.005sec.Over all the simulations have the same output voltage.

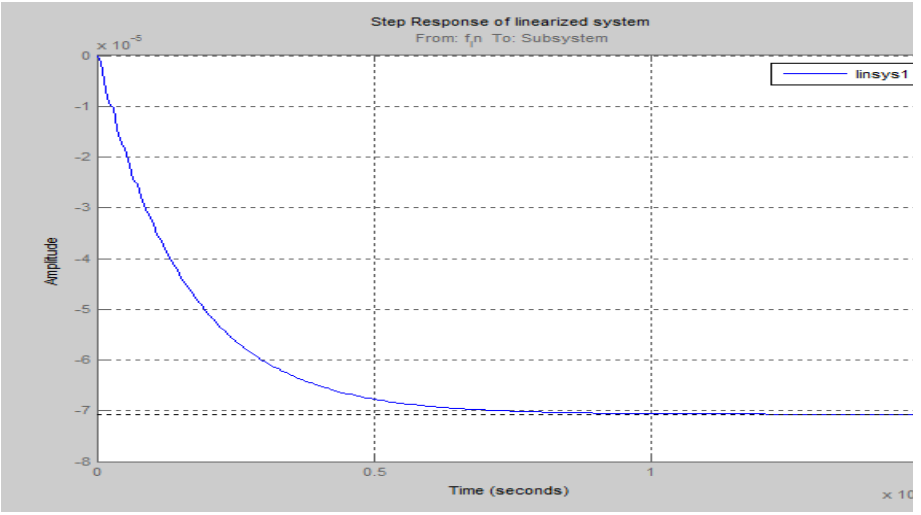

Fig.4- 7: step response of linear dynamic model

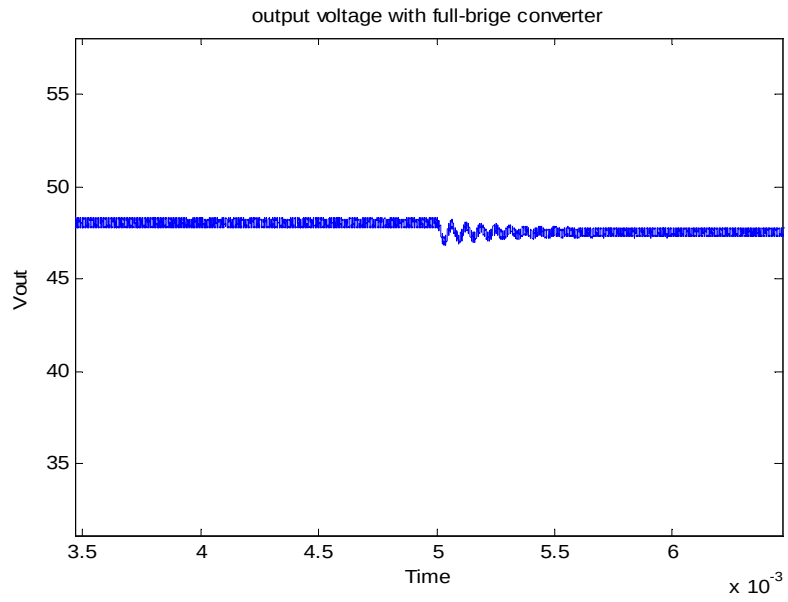

Fig.4- 8: Output voltage step response with full-bridge converter

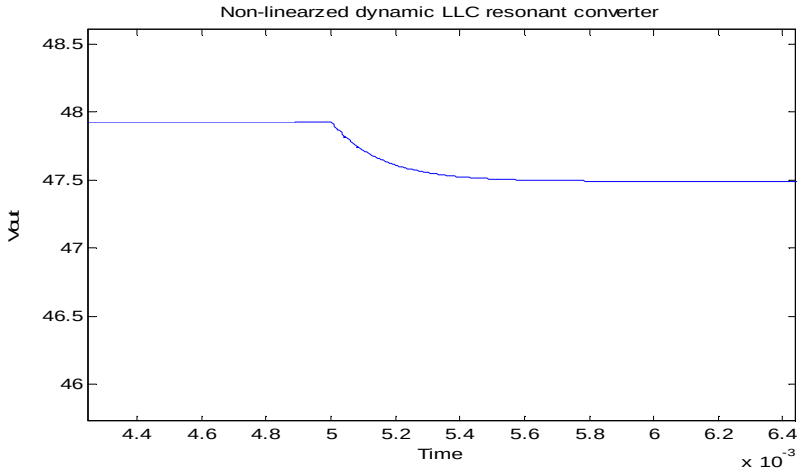

Fig.4- 9: Output voltage step response of the non-liberalized dynamic model

4.4.6 Control output Transfer function

The transfer function of the plant can be solved using mat lab from eq. (33) and (34) using mat lab code: *sys = ss(A, B, C, D).* The *ss* mat lab command arranges *A, B, C* and *D* matrices in state space response. Therefore the continuous s-transfer function of the plant can be given by the Mat Lab command as:

G_{pl}= *tf(sys)* and its zeros and poles can be stated as

G_{pl} = *tf(num, den)*

zpk(G_{pl}*)* from these mat lab commands the transfer function of the plant is shown in Equation 35.

$$G_p(s) = G_{pl}(s)G_F(s)$$

$$G_p(s) = \frac{-51.192\,(s-2.072e9)(s+5e6)(s-9.317e5)(s^2+1.214e5s+3.979e11)}{(s+6345)(s^2+2.69e4s+7.639e10)(s^2+7.968e6s+1.627e13)} * G_f \qquad (35)$$
$$(s^2+8.098e5s+1.86e12)\,(s^2+1.181e5s+3.983e11)\,(s^2+2.69e4s+9.617e11)$$

G_{pl} = transfer function of the converter, G_p = transfer function of the whole plant

$G_F(s)$ is Laplace-domain transfer function of the feedback. The feedback sub-system include the voltage sensor and noise filter capacitor. Its transfer function is developed from the voltage divider and the parallel connected capacitor.

$$G_F(s) = K_P \frac{1}{K_i s+1} \qquad (36)$$

where $K_P = 0.06\ and\ K_i = 3.183 * 10^{-4}$

$$G_p(s) = \frac{-964.98(s-2.072e09)(s+5e06)(s-9.317e05)(s^2+1.214e05s+3.979e11)}{(s+6345)(s+3142)(s^2+2.69e04s+7.639e10)(s^2+1.181e05s+3.983e11)} \qquad (37)$$
$$(s^2+8.098e05s+1.086e12)\,(s^2+7.968e06s+1.627e13)\,(s^2+2.69e04s+9.617e11)$$

In order to control the output it need to add compensator and feedback from output. Since the feedback is included in the plant, therefore the feedback has unity value. The compensated error for the operating points is acceptably selected from the plant and feedback transfer function using MATLAB command:

#opt = pidtuneOptions('CrossoverFrequency',2*pi*Fs)

#G_c = pidtune(H_s,'pid',opt)

From the command the suitable controller is PID controller with $K_p = 4.46*10^3$, $K_i = 1.29*10^7$ and $K_D = 82.7$

Therefore the s-transfer function is derived in equation 38.

$$G_c(s) = K_P + K_i\frac{1}{s} + K_D s \qquad (38)$$

$$G_c(s) = 4.46 * 10^3 + 1.29 * 10^7\frac{1}{s} + 82.7s$$

The open loop transfer function of the whole converter system including the compensator as shown in Fig.4-1 developed in the following steps.

$$G_{OL}(s) = \mathrm{G_p(s)G_c(s)}$$

$$G_{OL}(s) = \frac{\begin{matrix}79798\,(\mathrm{s}-2.072\mathrm{e}09)(\mathrm{s}+5\mathrm{e}06)(\mathrm{s}-9.317\mathrm{e}05)(\mathrm{s}+5.091\mathrm{e}04)(\mathrm{s}+3055)\\ (\mathrm{s}^2+1.214\mathrm{e}05\mathrm{s}+3.979\mathrm{e}11)(\mathrm{s}^2+8.098\mathrm{e}05\mathrm{s}+1.086\mathrm{e}12)\end{matrix}}{\begin{matrix}\mathrm{s}\,(\mathrm{s}+6345)(\mathrm{s}+3142)(\mathrm{s}^2+2.69\mathrm{e}04\mathrm{s}+7.639\mathrm{e}10)(\mathrm{s}^2+1.181\mathrm{e}05\mathrm{s}+3.983\mathrm{e}11)\\ (\mathrm{s\hat{}}2+7.968\mathrm{e}06\mathrm{s}+1.627\mathrm{e}13)(\mathrm{s\hat{}}2+2.69\mathrm{e}04\mathrm{s}+9.617\mathrm{e}11)\end{matrix}} \qquad (39)$$

The system response with small variation frequency or variation in load current expressed as transfer function that verifies a relationship between input and output variables. This can be described using the closed loop relation using the following general relation from Fig.4-1 diagram.

$$G_{CL}(s) = \frac{G_{OL}}{1+G_{OL}} \qquad (37)$$

$$G_{CL}(s) = \frac{\begin{matrix}79798\,s\,(s-2.072e09)(s+5e06)(s-9.317e05)(s+5.091e04)(s+6345)(s+3142)(s+3055)\\ (s^2+2.69e04s+7.639e10)(s^2+1.214e05s+3.979e11)(s^2+7.968e06s+1.627e13)\\ (s\hat{}2+1.181e05s+3.983e11)(s\hat{}2+8.098e05s+1.086e12)\,(s\hat{}2+2.69e04s+9.617e11)\end{matrix}}{\begin{matrix}s\,(s+6345)(s+3142)(s+3018)(s^2+7141s+3.607e07)(s^2+2.618e04s+7.631e10)\\ (s^2+2.69e04s+7.639e10)(s^2+7.968e06s+1.627e13)^2(s^2+1.181e05s+3.983e11)^2\\ (s\hat{}2+2.695e04s+9.617e11)\,(s\hat{}2+2.69e04s+9.617e11)\end{matrix}} \qquad (40)$$

4.4.7 Controlled output voltage

As described in the above simulation the step response of the converter is not controlled. The voltage output stay after the change of the frequency. But the goal of developing the control transfer function is to develop the controller in order to control the output voltage while the load changes. From Fig.4-9 indicates controlled output voltage with 48V at steady state. When a load change the compensator detect the error and feed to the controller and adjust the controller switching frequency in order to have constant voltage. The simulation result shows an increase of load at the load terminal, which result to reduce the output voltage as a result detect the error and finally adjust the switching frequency to approximately 99.5KHz to gate constant output voltage.

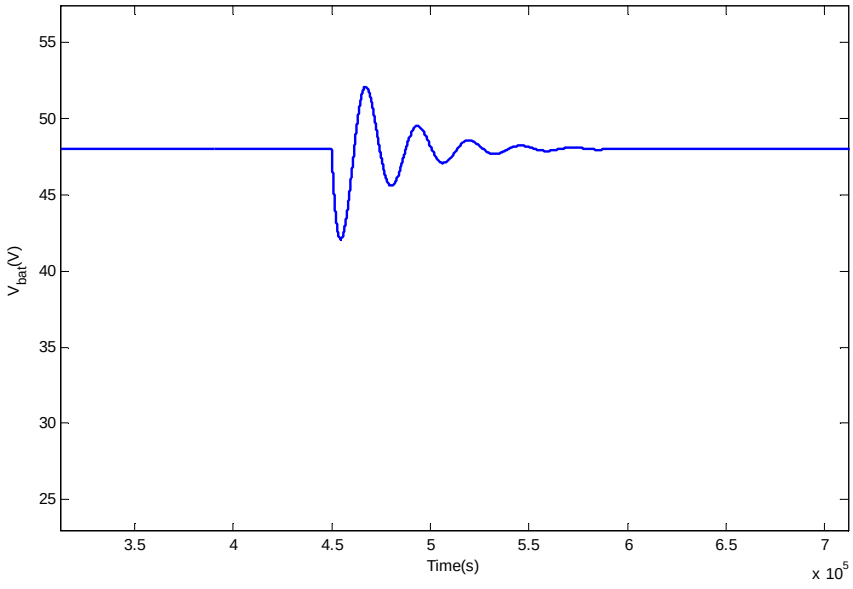

Fig.4- 10:Controlled output voltage

4.5 Small Signal Analysis For discharging Mode of Operation

The procedures to analysis the small signal model in step-up mode of operation is similar to the step-down mode of operation. Equivalent circuit of the converter is developed by reflecting circuit parameters to secondary of the isolated transformer using transformer turn ratio N. The detail analysis of each circuit component and equivalent circuit is similar as section 4.4.1, 4.4.2, 4.4.3 and 4.4.4. The detail analysis of the small signal for backward mode of operation is provided in appendix C.

4.5.1 States Space Equations For Backward Mode of Operation

The steps to develop for this state equations are similar to section 4.4.4. The details analysis is provided in the appendix B. The state space equations for backward mode of operation have the following expression which is similar to the forward mode of operation.

$$\frac{dx'}{dt} = Ax' + Bu' \qquad (33)$$

$$y' = Cx' + Du' \qquad (34)$$

Where $x' = (i_{ps}\ i_{pc}\ i_{ss}\ i_{sc}\ v_{ps}\ v_{pc}\ v_{ss}\ v_{sc}\ v_c)^T$ state variables of the system and A,B,C and D are matrix coefficient of the states.

$u = (\omega)$ control input which is frequency

$$A = 10^6 * \begin{bmatrix} -0.03 & 0 & 0 & 0.00 & 0.00 & 0 & 0 & 0.05 & 0.05 \\ 0 & 0 & 0 & 0.13 & 0.11 & 0.63 & 0 & 0 & 0 \\ 0 & 0 & 0 & 0.11 & 0.13 & 0 & 0.63 & 0 & 0 \\ 0 & -1.63 & 0 & 0 & 0 & 0 & 0 & 0.63 & 0.00 \\ 0 & 0 & -1.63 & -0.43 & -0.51 & 0 & 0 & 0.00 & 0.63 \\ 0 & -0.63 & 0 & 0 & 0 & 0 & 0 & 0.13 & 0.11 \\ 0 & 0 & -0.63 & 0 & 0 & 0 & 0 & 0.11 & 0.13 \\ 0 & 0 & 0 & -0.63 & 0.00 & -1.63 & 0 & 0 & 0 \\ 0 & 0 & 0 & -0.00 & -0.63 & 0 & -1.63 & -0.43 & -0.51 \end{bmatrix}$$

$$B = \begin{bmatrix} 0 \\ -10{,}95 \\ -0.0262 \\ 105.845 \\ 105.957 \\ -40.768 \\ -40.771 \\ -187.11 \\ 158.594 \end{bmatrix} \quad C = \begin{bmatrix} 0.9999 & 0 & 0 & 0.000 & 0 & 0 & 0 & 0.0002 & 0.0003 \end{bmatrix} \qquad D = [0]$$

4.5.2 Control output Transfer function

The relationship between the output voltage and compensator is the same as the forward mode of operation. The compensator error amplifier can be developed from converter plant. Therefore the resonant converter Laplace-domain transfer function is analyzed from the state space equation in section 5.5.1.The transfer function of the plant can be solved using mat lab commands as :

sys = ss(A, B, C, D). The ss mat lab command arranges A, B, C and D matrices in state space response. Therefore the continuous s-transfer function of the plant can be given by the Mat Lab command:

G_{pl}= tf(sys) and its zeros and poles can be stated as

G_{pl} = tf(num, den)

zpk(G_{pl}) from these mat lab commands the transfer function of the plant is shown in Equation 35.

$$G_p(s) = G_{pl}(s)G_F(s)$$

$$G_p(s) = \frac{\begin{matrix}-3.6733e{-}11\ (s{-}4.022e11)(s{-}9.793e08)(s{+}2e07)(s{-}2.112e05)\\ (s\text{^}2 + 1.632e05s + 1.897e11)(s\text{^}2 + 4.714e04s + 6.041e11)\end{matrix}}{\begin{matrix}(s{+}2666)\ (s\text{^}2 + 4.708e05s + 5.94e10)\ (s\text{^}2 + 3.851e04s + 1.981e11)\\ (s\text{^}2 + 3.851e04s + 6.597e11)\ (s\text{^}2 + 4.708e05s + 1.48e12)\end{matrix}} * G_f \qquad (41)$$

$G_F(s)$ is Laplace-domain transfer function of the feedback. The feedback is the voltage sensor with noise filter capacitor. Its transfer function is developed from the voltage divider and the parallel connected capacitor.

$$G_F(s) = K_P \frac{1}{K_i s+1} \qquad (42)$$

where $K_P = 0.06 \; and \; K_i = 3.183 * 10^{-4}$

$$G_p(s) = \frac{\begin{matrix}6.9243e{-}10\ (s{-}4.022e11)\ (s{-}9.793e08)\ (s{+}2e07)(s\hat{}2 + 1.632e05s + 1.897e11)\\ (s{-}2.112e05)(s\hat{}2 + 4.714e04s + 6.041e11)\end{matrix}}{\begin{matrix}(s{+}3142)\ (s{+}2666)\ (s\hat{}2 + 4.708e05s + 5.94e10)(s\hat{}2 + 3.851e04s + 1.981e11)\\ (s\hat{}2 + 3.851e04s + 6.597e11)(s\hat{}2 + 4.708e05s + 1.48e12)\end{matrix}} \qquad (43)$$

The compensated error for the operating points is acceptably selected from the plant and feedback transfer function using MATLAB command:

#opt = pidtuneOptions('CrossoverFrequency',2*pi*Fs)

#G_c = pidtune(H_s,'pid',opt)

From the command the suitable controller is PID controller with K_p = 1.49*10^6, K_i = 2.68*10^9 and K_D = 72.1

Therefore the s-transfer function is derived in equation 36.

$$G_c(s) = K_P + K_i \frac{1}{s} + K_D s \qquad (44)$$

$$G_c(s) = 1.49 * 10^6 + 2.68 * 10^9 \frac{1}{s} + 72.1s$$

The open loop transfer function of the system from the general diagram in Fig. 5-1

$$G_{OL}(s) = \mathrm{G_p(s)G_c(s)}$$

$$G_{OL}(s) = \frac{\begin{matrix}-5.0e{-}08\ (s{-}4.022e11)\ (s{-}9.793e08)\ (s{+}2e07)\ (s{-}2.112e05)\ (s{+}1.869e04)\\ (s{+}1993)(s\hat{}2 + 1.632e05s + 1.897e11)\ (s\hat{}2 + 4.714e04s + 6.041e11)\end{matrix}}{\begin{matrix}s\ (s{+}3142)\ \ (s\hat{}2 + 4.708e05s + 5.94e10)(s\hat{}2 + 3.851e04s + 1.981e11\\ (s\hat{}2 + 3.851e04s + 6.597e11)(s\hat{}2 + 4.708e05s + 1.48e12)\ (s{+}2666)\end{matrix}} \qquad (45)$$

The system response with small variation frequency or variation in load current expressed as transfer function that verifies a relationship between input and output variables. This can be described using the closed loop relation using the following general relation from Fig. 5-1 diagram.

$$G_{CL}(s) = \frac{G_{OL}}{1+G_{OL}} \qquad (45)$$

4.6 Frequency Response From Small Signal Analysis

Body plots are critical to determine the behavior of the frequency response of the resonant converter. The simulated bode plot of the control to output voltage transfer function based on the calculated circuit parameter from the design isolated bi-directional resonant converter derived in chapter 4. The controller, also called compensated error amplifier in both mode of operations are designed based on the transfer function of the converter plant.

The simulated body plot shows an open loop frequency response from the open loop transfer function of the compensated error amplifier and the plant of the isolated bidirectional resonant converter.

4.6.1 Bode plots for the forward mode of operation

In forward mode of operation the theoretical bode plot of the compensated to output transfer function is simulated in forward open loop operation. The compensated converter and uncompensated converter open loop transfer functions are included in the Fig. 4-12.

The parameters numerical values derived in chapter 4 and in small signal analysis in section 4.3-4.5 are used for the simulations. For the control to output transfer function, 400 V DC input voltage to 48 V DC with 62.5A load isolated bi-directional dc-dc resonant converter application.

The bode shown in Fig. 5-12 has a frequency crossover at 4.54 KHz in compensated resonant converter. The bode plot shows the system is closed loop stable. The theoretical bode plot shows the marginal gain is 31.1dB at 272 KHz frequency and also has phase marginal of 60^0

4.6.2 Bode plots for the backward mode of operation

In backward mode of operation the theoretical bode plot of the compensated to output transfer function is simulated in backward open loop operation. The compensated converter and uncompensated converter open loop transfer function are included in Fig. 5-13. The parameters, numerical values derived in chapter 4 and appendix are used for simulations. For control to output transfer function, 48 V DC input voltage to 400 V DC with 7.5A load isolated bi-directional dc-dc resonant converter application.

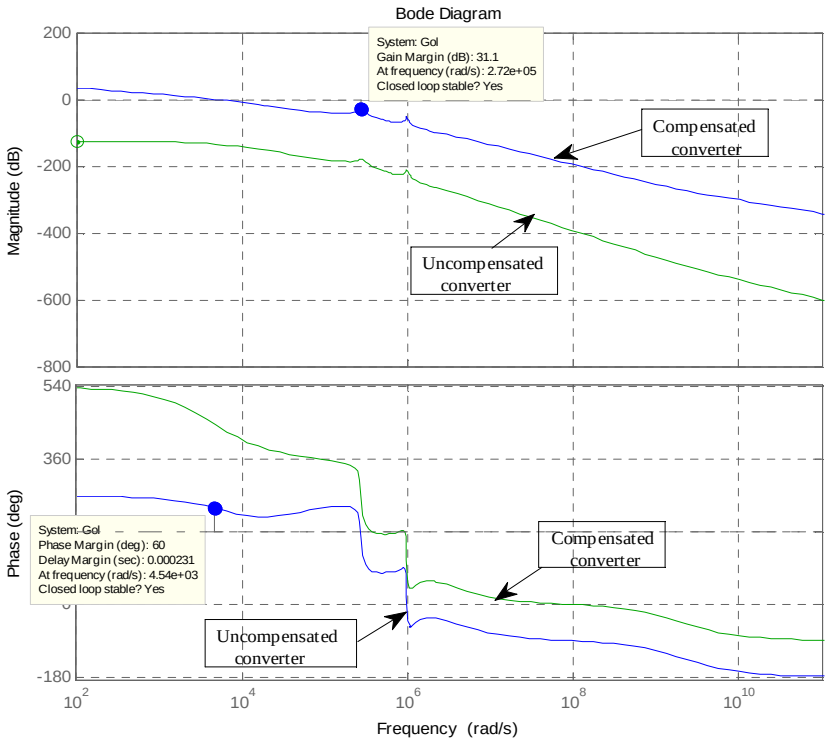

Fig.4- 11: Open loop bode plot for foreword mode

The theoretical bode plot indicates a frequency crossover at 4 KHz in compensated resonant converter. The bode plot shows the system is closed loop stable. The theoretical bode plot shows the marginal gain is 44.3dB at 130 KHz frequency and also has phase marginal of 60^0.

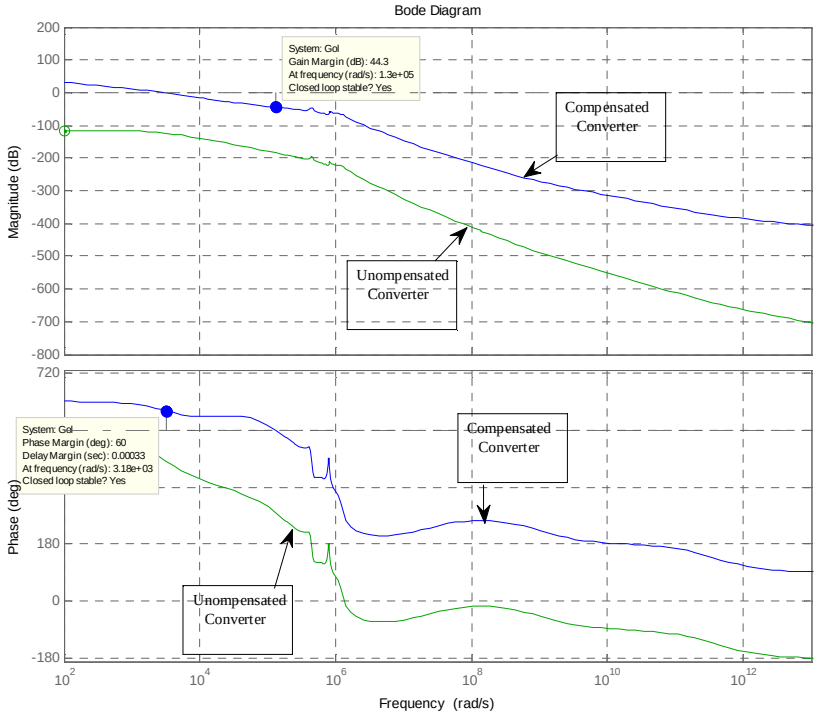

Fig.4- 12: Open loop bode plot for backward mode

Chapter 5- Designing Power Component And Controller

5.1 Filter design and analysis

Since Ac power are always available at low cost but not for DC power; therefore it need methods to change from AC to DC. This leads consumption of extra components at the dc terminal[51]. As described and sketched in chapter 3; both the charging and the discharging mode of operation bi-directional DC-DC LLC resonant converter has rectifier at their output. The output is full-wave rectified; then it is necessary to has filter at the output side in order to have DC output. Due to have high peak to peak or ripple value at output may have cause of heat loss and increase the temperature [52].

In general filters can be classified in to three main categories:

1 capacitor filter

2 inductor filter

3 combination of capacitor and inductor filters

For this topology design of bi-directional DC-DC LLC resonant converter is enough to use only capacitor filters. Because the power application is low 3KW, the capacitor has the ability to filter the ripple current as well as voltage much less than 3% which is the minimum requirement of the filter.

5.1.1 capacitor filter

As discussed in the simulation part of the two mode of operation the output of the rectifiers are full-wave voltage and current with very large ripples. The large fluctuation of the signals can be filtered using capacitor and reduce the ripple and stored in the capacitor and discharged by the load.

Fig.5-1 shows that the full-bridge rectifier of the resonant output signal of step-up or charging part of the last chapter simulation.

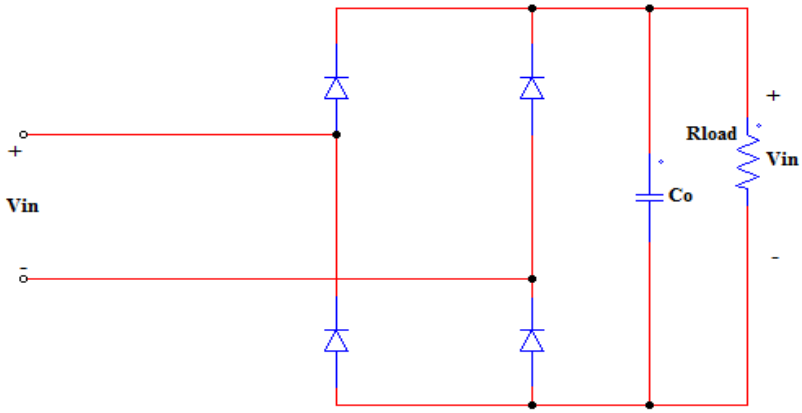

Fig.5- 1: The circuit design for full-bridge rectifier with capacitor filter

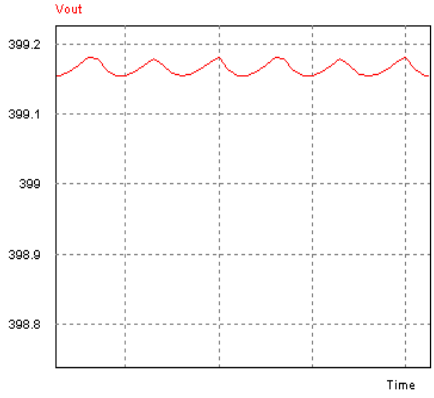

b. output voltage with capacitor filter

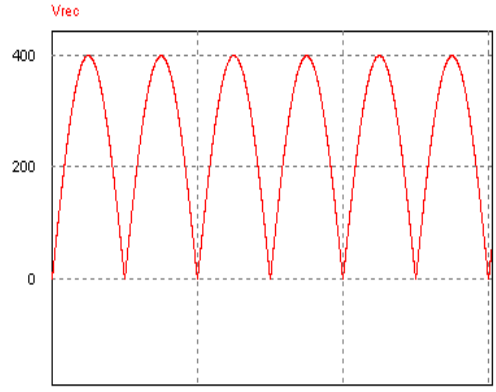

a. with out capacitor filter

Fig.5- 2: output voltage for both a)without and b) filter capacitor

The approximate sinusoidal output of the secondary resonant converter serves as a source to the full-bridge rectifier with amplitude 400V and 282.84V rms. As shown in figure 4.1 filter capacitor is represented by C and the load also represented by R_{load}. From Figure 4.2a the ripple of voltage is very high approximately 400; whereas the standard ripple value is less than or equal to $\Delta V=3\%$.

The voltage across the capacitor and the load is much enough filtered and its ripple value much less than 3% as shown in Figure 4.2b. Therefore it is critical to evaluate numerical analysis for capacitor magnitude for the given specifications and selected ripple value. Even though it is common to select ripple factor RF≤3%, but there is a generalized equation to calculate the ripple factor[52].

$$Rf = \frac{1}{\sqrt{2}(2frRC-1)} \qquad (1)$$

Where R is the load resistance

fr resonant frequency

C capacitor

Then it is possible to analysis the value of Capacitor for the given specified parameters, From the given power 3KW and output voltage 400V we can calculate the load resistance 53.33Ω and given 100KHz resonant frequency. To have a more accurate dc output you need to select less ripple factor less than 1%, let us take Rf = 0.1% . But value of the resonant frequency is doubled because the rectifier is full-bridge so it doubles the frequency of the rectified as well as filtered output.

From equation 1

$$C = \frac{\frac{1}{\sqrt{2}Rf} + 1}{2frR}$$

$$C = \frac{\frac{1}{\sqrt{2} * 0.001} + 1}{2 * 2 * 100000 * 53.33}$$

$$C = 127\mu F$$

5.2 Design of LLC resonant components

Growing the application and demand of the LLC resonant converter as mentioned in chapter 2 in its half bridge is necessary to study how to analysis each component in relation to the given specification of the converter. The purpose of this sub-topic is a qualitative detail analysis at steady-state operation of full-bridge converter topology which is similar to the half-bridge topology converter. In general more detail step of the analysis for the LLC component is developed in the reference[53]; but here will discuss the most common design procedure.

5.2.1 Design procedure for LLC analysis

The most basic detail step by step design procedure for calculating the parameters of the LLC resonant converter has been defined from [53]. From the given specification and using the following ten steps we can calculate the values of : resonant inductor, resonant capacitor and magnetizing resonant converter.

Procedure 1. Design specifications

- Input voltage range: $V_{dc.min}$ - $V_{dc.max}$
- Nominal input voltage: $V_{dc.nom}$
- Output voltage: V_{out}
- Output power: P_{out}
- Resonant frequency: f_r
- Maximum operating frequency: f_{max}
- Parasitic capacitance from node to neutral N: C_{ZVS}
- Dead time of driving circuit: T_D

Procedure 2. General criteria for the design

- The design will be assumed for the converter at the operating of resonance and nominal input voltage
- The resonant converter must always work at ZVS in the whole operating system

Procedure 3. the ten step to analysis the LLC resonant components

Step-1: calculate the transformer turn-ratio

$$n = \frac{\text{Vdc.nom}}{\text{Vout}}$$

Step-2: calculate the maximum and minimum require gains at the extreme values of the input voltage range

$$Mmax = n\frac{\text{Vdc.max}}{\text{Vout}}$$

$$Mmin = n\frac{\text{Vdc.min}}{\text{Vout}}$$

Step-3: calculate the maximum normalized operated frequency

$$fnmax = \frac{\text{fmax}}{\text{fr}}$$

Step-4: calculate the inductance ratio by assuming the converter is under the maximum frequency at zero load and maximum input voltage

$$\lambda = \frac{1-Mmin}{\text{Mmin}}\frac{fnmax^2}{fnmax^2-1}$$

Step-5: calculating the effective load resistance reflected at the primary side of the transformer

$$Rac = \frac{2\text{n}^2\text{Vout}^2}{\pi^2 Pout}$$

Step-6: evaluating the maximum Q characteristic in the operation of ZVS region at minimum input voltage and full load condition

$$Qzvs' = 0.95Qmax = 0.95\frac{\lambda}{\text{Mmax}}\sqrt{\frac{1}{\lambda}+\frac{Mmax^2}{Mmax^2-1}}$$

Step-7: evaluating the maximum Q characteristic in the operation of ZVS region at maximum input voltage and no-load condition

$$Qzvs'' = \frac{2\lambda fnmax.Td}{\pi\left((\lambda+1)\text{fnmax}^2-\lambda\right)RacCzvs}$$

Step-8: choose the best characteristic ZVS quality control in the operating range such that:

$$Q_{ZVS} \leq \min\{ Q_{ZVS'}, Q_{ZVS''} \}$$

Step-9: calculate the minimum operating frequency at full-load and minimum input voltage

$$f_{min} = fr \sqrt{\frac{1}{1+\frac{1}{\lambda}\left(1-\frac{1}{Mmax^{1+\frac{Qzvs}{Qmax}^4}}\right)}}$$

Step-10: calculating the characteristic impedance of resonant tank and calculate each parameters of the resonant tank.

$$Z_O = Q_{ZVS}R_{ac}$$

$$Cr = \frac{1}{2\pi frZo}$$

$$Lr = \frac{Zo}{2\pi fr}$$

$$Lm = \frac{Zo}{2\pi fr\lambda} = \frac{Lr}{\lambda}$$

Based on the above procedures it is possible to calculate the resonant tanks on both sides of the dual full-bridge LLC resonant converter. The calculation is classified in two ways:

A. Design LLC resonant component for primary side

Procedure 1. Design specifications

- Input voltage range: 380V - 420V
- Nominal input voltage: 400V
- Output voltage: 48V
- Output power: 3KW
- Resonant frequency: 100KHz
- Maximum operating frequency: 150KHz
- Parasitic capacitance from node to neutral N: C_{ZVS} = 350pF
- Dead time of driving circuit: T_D = 270ns

therefore from the above steps of procedure 3 is easy to calculate the value of parameters:

step-1: n = 8.33

step-2: M_{max} = 1.05 M_{min} = 0.952

Step-3: $f_{nmax} = 1.5$

Step-4: $\lambda = 0.0907$

step-5: $R_{ac} = 10\text{-}81\Omega$

Step-6: $Q_{ZVS'} = 0.3769$

Step-7: $Q_{ZVS''} = 2.70$

Step-8: $Q_{ZVS} \leq 0.3769$

Step-9: $Z_o = 4.074\Omega$

step-10: $C_r = 391nF$ $L_r = 6.5\mu H$ $L_{mr} = 71.5\ \mu H$

B. Design LLC resonant component for secondary side

Procedure 1. Design specifications

- Input voltage range: 45.6V - 50.4V
- Nominal input voltage: 48V
- Output voltage: 400V
- Output power: 3KW
- Resonant frequency: 100KHz
- Maximum operating frequency: 150KHz
- Parasitic capacitance from node to neutral N: $C_{ZVS} = 350pF$
- Dead time of driving circuit: $T_D = 270ns$

  therefore from the above steps of procedure 3 is easy to calculate the value of parameters:

  step-1: $n = 0.120048$

  step-2: $M_{max} = 1.05$ $M_{min} = 0.952$

  Step-3: $f_{nmax} = 1.5$

  Step-4: $\lambda = 0.0907$

  step-5: $R_{ac} = 0.155\Omega$

  Step-6: $Q_{ZVS'} = 0.3769$

  Step-7: $Q_{ZVS''} = 2.70$

  Step-8: $Q_{ZVS} \leq 0.3769$

  Step-9: $Z_o = 0.0584\Omega$

  step-10: $C_r = 27.25\mu F$ $L_r = 93nH$ $L_{mr} = 1\mu H$

5.3 Gate driver design

Fig. 5-3 shows the H-bridge gate driver selected and its topology for half-bridge MOSFETs control circuit. IR2110 is the selected gate driver due to its specification which is compatible with this bidirectional dc-dc resonant converter. IR2110 is high voltage, high speed power MOSFET's driver with high and law side reference input and output channels[54].

Symbol	Definition	Min	Max	Unit
V_b	High side floating supply voltage	-0.3	525	V
V_s	High side floating supply offset voltage	V_b-25	V_b+0.3	
V_{Ho}	High side floating output voltage	V_s-0.3	V_b+0.3	
V_{cc}	Low side fixed supply voltage	-0.3	25	
V_{Lo}	Low side output voltage	-0.3	V_{cc}+0.3	
V_{dd}	Logic supply voltage	-0.3	V_{ss}+25	
V_{ss}	Logic supply offset voltage	V_{cc}-25	V_{cc}+0.3	
V_{in}	Logic input voltage (H_{in}, L_{in} and SD)	V_{ss}-0.3	V_{dd}+0.3	
dV_s/dt	Allowable offset supply voltage transient	-----	50	V/ns
P_d	Package power dissipation Ta≤ +25	-----	1.6	W
R_{THJA}	Thermal resistance, junction to ambient	-----	75	^{0}C/W
T_J	Junction temperature	-----	150	^{0}C
T_S	Storage temperature	-55	150	

Table 1 Absolute Maximum rating information of IR2110

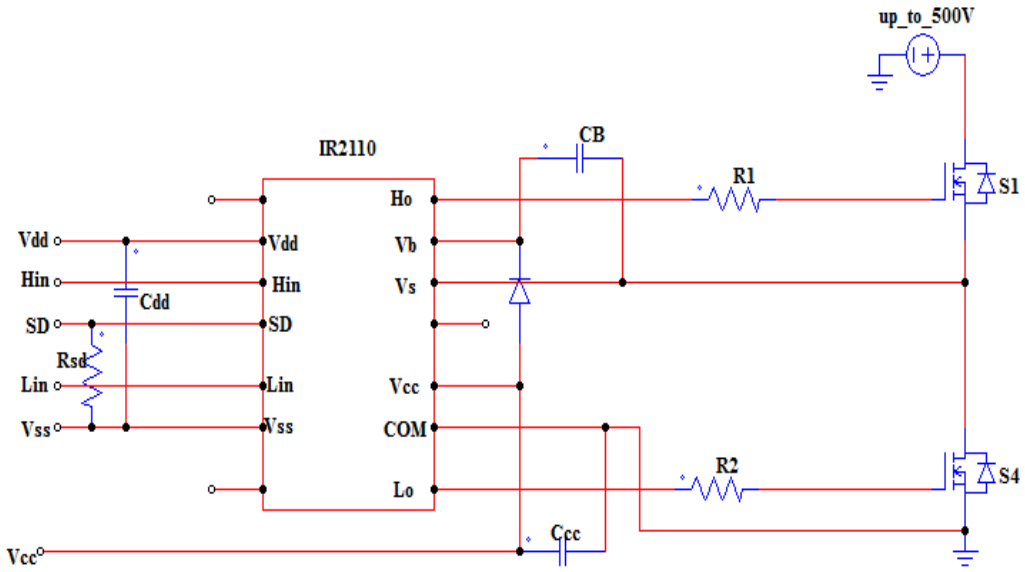

Fig.5- 3: Gate driver circuit design for half-bridge switch control

The gate driver circuit components are selected based on the specification of MOSFETs, application type and the noise considerations. SD is the shutdown signal which has signal with amplitude of zero. Since the switching frequency is very large, the gate driver signals can be disturbed. Therefore R_{SD} which a value in 56KΩ drops the noise from the surrounding in SD channel. R_1 and R_2 are series resistance to gate terminal of switches with 5W power rate. These resistors safe the MOSFETs during overshoot of voltage from gate driver. C_{CC} is the decoupling capacitor applicable for compensating the inductance supplied from the supply voltage V_{CC}.

5.3.1 How to select the bootstrap component

As shown Fig.5-3 bootstrap diode and capacitors are the only critical and external components to generate the PWM signals for the MOSFETs operation. The selection of bootstrap component depends on the MOSFET and MOS-gate driver.

The voltage that supply to bootstrap capacitor is V_{CC}. The capacitance of bootstrap capacitor is determined by the following specifications[55]:

1. Gate voltage required to enhance MOSFET gate driver
2. I_{QBS} -quiescent current for the high-side driver circuitry
3. Current within the level shifter of the controller I_C
4. MOS-gate driver gate-source forward leakage current

5. Bootstrap capacitor leakage current

These are the general factors for selecting the bootstrap electrolytic capacitor, but for non-electrolytic capacitors have the following general equation.

$$Q_{bs} = 2Q_g + \frac{I_{qbs(max)}}{f} + Q_{ls} + \frac{I_{cbs(leak)}}{f}$$

$$C_{bs} \geq \frac{2 * \left[2Q_g + \frac{I_{qbs(max)}}{f} + Q_{ls} + \frac{I_{cbs(leak)}}{f}\right]}{V_{cc} - V_f - V_{LS} - V_{Min}}$$

where:

Q_g = Gate charge of high side of FET

Q_{bs} = Gate charge from bootstrap to source

f = Switching frequency

$I_{cbs(leak)}$ = Bootstrap capacitor leakage current

$I_{qbs(max)}$ = Maximum V_{BB} quiescent current

V_{cc} = Logic section voltage source

V_f = Forward voltage drop across the bootstrap diode

V_{LS} = Voltage drop across the low side FET

V_{min} = Minimum voltage between V_b and V_s

Q_{ls} = Level shift charge required per cycle (typically 5nC for 500V)

Therefore from the data sheet of IR2110 gate driver and 2SK4012(Q) MOSFET the bootstrap capacitor is selected from the analysis.

f = 150KHz

$I_{qbs(max)}$ = 230µA $I_{cbs(leak)}$ = 0 (very low)

Q_g = 30nC Q_{ls} = 5nC

$V_{min} = 10V$ $V_f = 0.5V$

$V_{LS} = 2.5V$ $V_{cc} = 15V$

So that from the above equation:

$$C_{bs} \geq 0.44\mu C$$

But from practical application and implementation, most of time it is recommended to multiply the calculated value with four just for safety.

Chapter-6: Experimental results

6.1 Introduction

This chapter discusses the practical result of the galvanic isolated bidirectional DC-DC resonant converter. This experimental result provides for the charging(step-down) verific for the resonant converter with the one developed PCB is constructed where its sche diagram shown in Appendix E.

6.2 Charging mode

6.2.1 Experimental waveforms

Fig.6-1 shows that the isolated bidirectional DC-DC LLC resonant converter in chargi step-down mode of operation. The important test points for this experimental results are shown in the following figures. The bi-directional LLC resonant converter shown in Fi has been tested for 100V input and around 25V output voltage.

The experiment take for 9.9W test, 100V input voltage and 72.5Ω resistor load with 15/4 ratio high switching transformer and 134.4KHz switching frequency of the controlling drive signal.

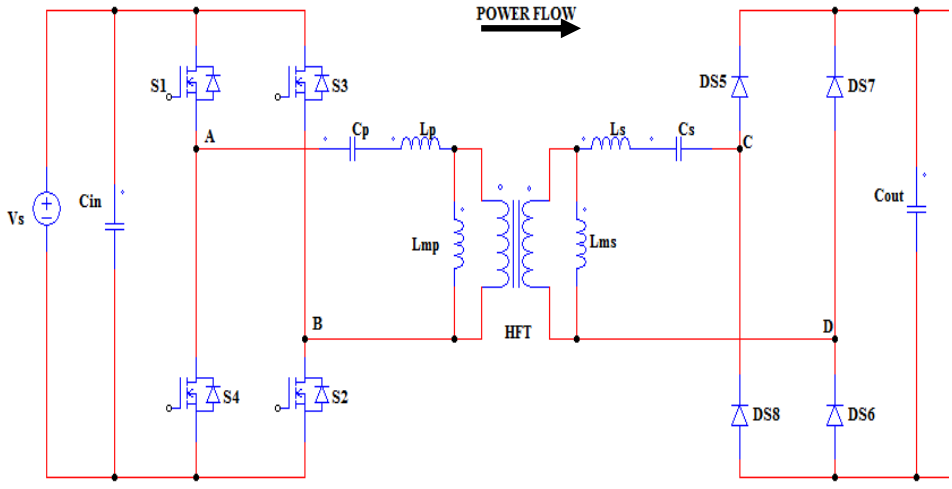

Fig.6- 1: Converter in discharging mode of operation

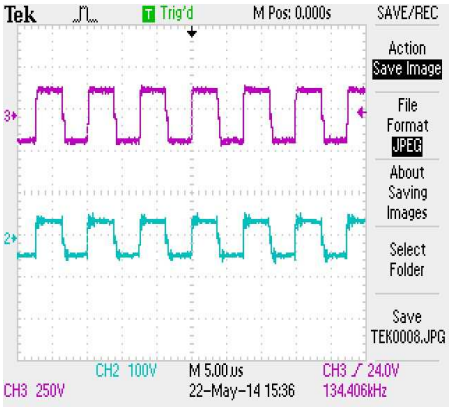

a) V_{ab} and V_{cd}

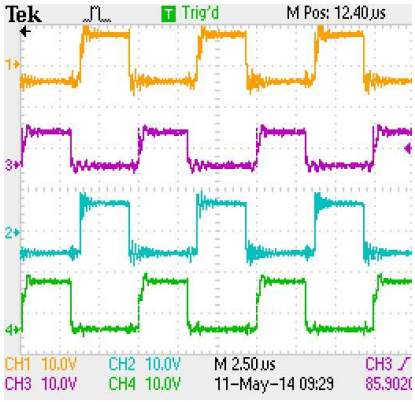

b) gate drive signals

Fig.6- 2: a) CH1: V_{ab} 250V/div, CH2: V_{cd}, and b) CH1 and CH2 are gate driver sign S1 and S2 and CH3 and CH4 to S3 and S4 respectively with 10V/div

The output voltage of the primary bridge is shown in the Fig.6-2. As it shown in the Fi the gate drive signal have not 0.5 duty cycle due to dead time of the MOSFETs. Ther from the specification of the switches calculation the controller generate the signals with cycle less than 0.5 value and its duty cycle value is around 0.45. The gate source voltag values are shown in the Fig.6-2 with in part (b) is approximately 15V which is enou switch-on the MOSFETs.

Fig.7-3 shows that the secondary voltage V_{cd} have a peak value around 24.4V and C average output current with 100V input voltage, 72.5Ω resistor load, 15/4 transformer ratio and the switching frequency of the gate driver signal is 134.4KHz.

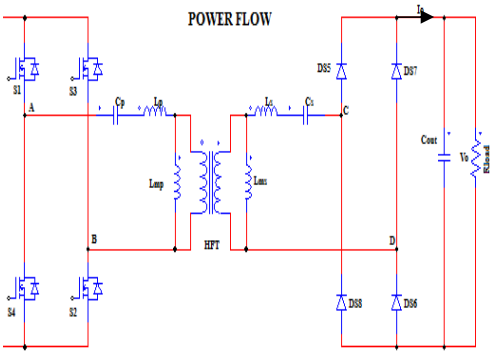

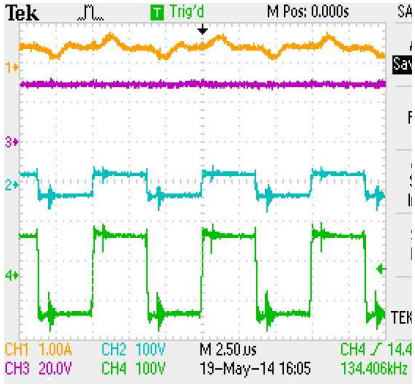

Fig.6- 3 CH1: Io 1A/div, CH2: Vcd 100V/div, CH3: Vo 25V/div and CH4: Vab 100V/div

Chapter-7: Conclusion and Recommendations for future work

7.1 Conclusion

This report has presented isolated bidirectional DC-DC LLC resonant converter for multi-propose application. The proposed topology is compacted and combination of isolated bidirectional DC-DC converter with LLC resonant tank which characterizes the power to flow in both direction. The converter unit has a high switching frequency transformer and purposed for galvanic isolation between the high voltage side with low voltage side or battery but load for this thesis.

This presented isolated bidirectional DC-DC LLC resonant converter concerns the converter to include dual active bridge switches with transformer isolation. The full-bridge on the high side is called voltage-fed bridge and also the full-bridge on the low side is named as current-fed bridge. The simulation results of the isolated bidirectional DC-DC LLC resonant converter for both charging and discharging shows an efficiency of 97%. But from the laboratory result shows that the efficiency of the converter is approximately 95%.

This presented bidirectional dc-dc converter also contains detail analysis for small signal approach to develop the controlling system of the converter and also a controller is developed for automatic control of the power flow when a fault exist in utility. It is also developed a new approach for selecting the resonant tank parameters value by developing C-code programming which interface with the output values of the simulink results.

7.2 Suggestion for future works

The following suggestions are proposed for further work in isolated bidirectional DC-DC LLC resonant converter. One of the best way to solve the harmonic disturbance developed from switch can be solved by developing IME filter. Develop laboratory setups for automatic bidirectional controller during interruption of power from utility. This leads to shift the switching operation from charging mode of operation to discharging mode of operation in order to stay the converter operating.

Reference

[1] Chiu, H. J., & Lin, L. W. (2006). A bidirectional DC-DC converter for fuel cell electric vehicle driving system. *Power Electronics, IEEE Transactions on*, *21*(4), 950-958.

[2] Thomas, S., De Doncker, R. W., & Lenke, R. (2012). *U.S. Patent Application 14/002,593*.

[3] Inoue, S., & Akagi, H. (2007). A bidirectional DC–DC converter for an energy storage system with galvanic isolation. *Power Electronics, IEEE Transactions on*, *22*(6), 2299- 2306.

[4] Lee, Y. S., & Chiu, Y. Y. (2005, November). Zero-current-switching switched capacitor bidirectional DC-DC converter. In *Electric Power Applications, IEE Proceedings-* (Vol. 152, No. 6, pp. 1525-1530). IET.

[5] Rathore, A. K., Bhat, A. K., & Oruganti, R. (2012). Analysis, design and experimental results of wide range ZVS active-clamped LL type current-fed DC/DC converter for fuel cells to utility interface. *Industrial Electronics, IEEE Transactions on*, *59*(1), 473- 485.

[6] Kim, I. D., Paeng, S. H., Ahn, J. W., Nho, E. C., & Ko, J. S. (2007, June). New bidirectional ZVS PWM sepic/zeta DC-DC converter. In *Industrial Electronics, 2007. ISIE 2007. IEEE International Symposium on* (pp. 555-560). IEEE.

[7] Das, P., Mousavi, S., & Moschopoulos, G. (2010). Analysis and design of a non-isolated bidirectional ZVS-PWM DC–DC converter with coupled inductors. *Power Electronics IEEE Transactions on*, *25*(10), 2630-2641.

[8] Peng, F. Z., Li, H., Su, G. J., & Lawler, J. S. (2004). A new ZVS bidirectional DC-DC converter for fuel cell and battery application. *Power Electronics, IEEE Transactions on*, *19*(1), 54-65.

[9] Inoue, S., & Akagi, H. (2007). A bidirectional DC–DC converter for an energy storage system with galvanic isolation. *Power Electronics, IEEE Transactions on*, *22*(6), 2299- 2306.

[10] Karshenas, H. R., Daneshpajooh, H., Safaee, A., Bakhshai, A., & Jain, P. (2011, February). Basic families of medium-power soft-switched isolated bidirectional dc-dc converters. In *Power Electronics, Drive Systems and Technologies Conference (PEDSTC), 2011 2nd* (pp. 92-97). IEEE.

[11] Himmelstoss, Felix A. "Analysis and comparison of half-bridge bidirectional DC-DC converters." In *Power Electronics Specialists Conference, PESC'94 Record., 25th Annual IEEE*, pp. 922-928. IEEE, 1994.

[12] Yamamoto, Koji, Eiji Hiraki, Toshihiko Tanaka, Mutsuo Nakaoka, and Tomokazu Mishima. "Bidirectional DC-DC converter with full-bridge/push-pull circuit for automobile electric power systems." In *Power Electronics Specialists Conference, 2006. PESC'06. 37th IEEE*, pp. 1-5. IEEE, 2006.

[13] Jain, Manu, Matteo Daniele, and Praveen K. Jain. "A bidirectional dc-dc converter topology for low power application." *Power Electronics, IEEE Transactions on* 15, no. 4 (2000): 595-606.

[14] Kheraluwala, M. N., Randal W. Gascoigne, Deepakraj M. Divan, and Eric D. Baumann. "Performance characterization of a high-power dual active bridge dc-to-dc converter." *Industry Applications, IEEE Transactions on* 28, no. 6 (1992): 1294-1301.

[15] Dong Tan, F. "Maintaining soft switching in a phase-shifted bipolar DC-to-DC converter." In *Applied Power Electronics Conference and Exposition, 1997. APEC'97 Conference Proceedings 1997., Twelfth Annual*, vol. 2, pp. 783-789. IEEE, 1997.

[16] De Doncker, Rik WAA, Deepakraj M. Divan, and Mustansir H. Kheraluwala. "A three-phase soft-switched high-power-density DC/DC converter for high-power applications." *Industry Applications, IEEE Transactions on* 27, no. 1 (1991): 63-73.

[17] Xu, Dehong, Chuanhong Zhao, and Haifeng Fan. "A PWM plus phase-shift control bidirectional DC-DC converter." *Power Electronics, IEEE Transactions on* 19, no. 3 (2004): 666-675.

[18] Patella, Benjamin J., Aleksandar Prodic, Art Zirger, and Dragan Maksimovic. "High-frequency digital PWM controller IC for DC-DC converters." *Power Electronics, IEEE Transactions on* 18, no. 1 (2003): 438-446.

[19] Zhou, Siyuan, and Gabriel A. Rincón-Mora. "A high efficiency, soft switching DC-DC converter with adaptive current-ripple control for portable applications."*Circuits and Systems II: Express Briefs, IEEE Transactions on* 53, no. 4 (2006): 319-323.

[20] Bai, Hua, and Chris Mi. "Eliminate reactive power and increase system efficiency of isolated bidirectional dual-active-bridge DC–DC converters using novel dual-phase-shift control." *Power Electronics, IEEE Transactions on* 23, no. 6 (2008): 2905-2914.

[21] Hua, Guichao, Ching-Shan Leu, Yimin Jiang, and Fred CY Lee. "Novel zero-voltage-transition PWM converters." *Power Electronics, IEEE Transactions on*9, no. 2 (1994): 213-219.

[22] Tao, H., A. Kotsopoulos, J. L. Duarte, and M. A. M. Hendrix. "Multi-input bidirectional DC-DC converter combining DC-link and magnetic-coupling for fuel cell systems." In *Industry Applications Conference, 2005. Fourtieth IAS Annual Meeting. Conference Record of the 2005*, vol. 3, pp. 2021-2028. IEEE, 2005.

[23] Yang, Bo. *Topology investigation for front end DC/DC power conversion for distributed power system*. Diss. Virginia Polytechnic Institute and State University, 2003.

[24] Chiu, Huang-Jen, and Li-Wei Lin. "A bidirectional DC-DC converter for fuel cell electric vehicle driving system." *Power Electronics, IEEE Transactions on* 21.4 (2006): 950-958.

[25] Nagendrappa, H., and A. K. S. Bhat. "A fixed-frequency LCL-type series resonant converter with capacitive output filter using a modified gating scheme."*Power Electronics and Drive Systems (PEDS), 2013 IEEE 10th International Conference on*. IEEE, 2013.

[26] Kang, Y-G., and Anand K. Upadhyay. "Analysis and design of a half-bridge parallel resonant converter." *Power Electronics, IEEE Transactions on* 3.3 (1988): 254-265.

[27] Chuang, Ying-Chun, et al. "Analysis and implementation of half-bridge series–parallel resonant converter for battery chargers." *Industry Applications, IEEE Transactions on* 47.1 (2011): 258-270.

[28] Lin, Ray-Lee, and Chiao-Wen Lin. "Design criteria for resonant tank of LLC DC-DC resonant converter." *IECON 2010-36th Annual Conference on IEEE Industrial Electronics Society*. IEEE, 2010.

[29] Deboy, G., et al. "A new generation of high voltage MOSFETs breaks the limit line of silicon." *Electron Devices Meeting, 1998. IEDM'98. Technical Digest., International*. IEEE, 1998.

[30] Person, Clark. *Selection of Primary Side Devices for LLC Resonant Converters*. Diss. Virginia Polytechnic Institute and State University, 2008.

[31] Mohan, Ned, and Tore M. Undeland. *Power electronics: converters, applications, and design*. John Wiley & Sons, 2007.

[32] Lazar, James F., and Robert Martinelli. "Steady-state analysis of the LLC series resonant converter." *Applied Power Electronics Conference and Exposition, 2001. APEC 2001. Sixteenth Annual IEEE*. Vol. 2. IEEE, 2001.

[33] Batarseh, Issa. "Resonant converter topologies with three and four energy storage elements." *Power Electronics, IEEE Transactions on* 9.1 (1994): 64-73.

[34] Li, R., Pottharst, A., Frohleke, N., & Bocker, J. (2004, June). Analysis and design of improved isolated full-bridge bidirectional DC-DC converter. In *Power Electronics Specialists Conference, 2004. PESC 04. 2004 IEEE 35th Annual*(Vol. 1, pp. 521-526). IEEE.

[35] Jiang, Tianyang, Junming Zhang, Xinke Wu, Kuang Sheng, and Y. Wang. "A Bidirectional LLC Resonant Converter with Automatic Forward and Backward Mode Transition." (2014): 1-1.

[36] Halim, Mazliza Abdul, Muhamad Nabil Hidayat, and Mohammad Nawawi Seroji. "Implementation and analysis of a half-bridge series-parallel LLC loaded resonant DC-DC converter for low power applications." In *Power Electronics and Drive Systems (PEDS), 2013 IEEE 10th International Conference on*, pp. 634-638. IEEE, 2013.

[37] Cho, Jung-Goo, Juan A. Sabate, Guichao Hua, and Fred C. Lee. "Zero-voltage and zero-current-switching full bridge PWM converter for high-power applications." *Power Electronics,IEEE Transactions on* 11, no. 4 (1996): 622-628.

[38] Chen, Wei, Siran Wang, Xiaoyuan Hong, Zhengyu Lu, and Shaoshi Ye. "Fully soft-switched bidirectional resonant dc-dc converter with a new CLLC tank." In*Applied Power Electronics Conference and Exposition (APEC), 2010 Twenty-Fifth Annual IEEE*, pp. 1238-1242

[39] Narasimharaju, B. L., S. P. Dubey, and S. P. Singh. "Modeling and stability analysis of coupled inductor bidirectional DC-DC converter." In *Electron Devices and Solid-State Circuits (EDSSC), 2010 IEEE International Conference of*, pp. 1-5. IEEE, 2010.

[40] Cavalcante, F. da S., and Johann W. Kolar. "Small-signal model of a 5kW high-output voltage capacitive-loaded series-parallel resonant DC-DC converter." In *Power Electronics Specialists Conference, 2005. PESC'05. IEEE 36th*, pp. 1271-1277. IEEE, 2005.

[41] Maksimović, Dragan, and Regan Zane. "Small-signal discrete-time modeling of digitally controlled DC-DC converters." In *Proc. IEEE COMPEL Workshop*, pp. 16-19. 2006.

[42] de Groot, Humphrey, Eric Janssen, Rosario Pagano, and Kees Schetters. "Design of a 1-MHz LLC resonant converter based on a DSP-driven SOI half-bridge power MOS module." *Power Electronics, IEEE Transactions on* 22, no. 6 (2007): 2307-2320.

[43] Power Electronic text book

[44] Yang, Bo. "Topology investigation for front end DC/DC power conversion for distributed power system." PhD diss., Virginia Polytechnic Institute and State University, 2003.

[45] Chang, Chien-Hsuan, En-Chih Chang, Chun-An Cheng, Hung-Liang Cheng, and Sheng-Chang Lin. "Small signal modeling of LLC resonant converters based on extended describing function." In *Computer, Consumer and Control (IS3C), 2012 International Symposium on*, pp. 365-368. IEEE, 2012.

[46] Zhang, B., and M. H. Pong. "Dynamic model and small signal analysis based on the extended describing function and Fourier series of a novel AM ZVS direct coupling DC/DC converter." In *Power Electronics Specialists Conference, 1997. PESC'97 Record., 28th Annual IEEE*, vol. 1, pp. 447-452. IEEE, 1997.

[47] Emadi, Ali, Alireza Khaligh, Claudio H. Rivetta, and Geoffrey A. Williamson. "Constant power loads and negative impedance instability in automotive systems: definition, modeling, stability, and control of power electronic converters and motor drives." *Vehicular Technology, IEEE Transactions on* 55, no. 4 (2006): 1112-1125.

[48] Fernandez, Luis M., et al. "Hybrid electric system based on fuel cell and battery and integrating a single dc/dc converter for a tramway." *Energy Conversion and Management* 52.5 (2011): 2183-2192.

[49] Yang, Sihun, et al. "Dynamic characteristics model of bi-directional DC-DC converter using state-space averaging method." *Telecommunications Energy Conference(INTELEC), 2012 IEEE-34th International*. IEEE, 2012.

[50] Segaran, Dinesh, Donald Grahame Holmes, and Brendan Peter McGrath. "Enhanced load step response for a bidirectional dc–dc converter." *Power Electronics, IEEE Transactions on* 28.1 (2013): 371-379.

[51] Jeon, S. J., et al. "A primary-side-assisted zero-voltage and zero-current switching three-level DC-DC converter with phase-shift control." *Applied Power Electronics Conference and Exposition, 2002. APEC 2002. Seventeenth Annual IEEE*. Vol. 2. IEEE, 2002.

[52] Pyakuryal, Sudeep, and Mohammad Matin. "Filter Design for AC to DC Converter." *International Refereed Journal of Engineering and Science* 2.6 (2013): 42-49.

[53] Hung, Chia-Cheng. "Design and Implementation of a 2.4-kW Isolated Dual-Output AC-DC Converter." (2012).

[54] Zhao, Jingbo, et al. "Design and full-car tests of electric power steering system."*Computer And Computing Technologies In Agriculture, Volume I*. Springer US, 2008. 729-736.

[55] ICs, HV Floating MOS-Gate Driver. "*Application Note AN-978." Rev D* (2007).

APPENDIX

Appendix A1

```
%% The general code developed to generates
% value for the parameter of the resonant tank
% (i.e. Lp, Cp, Ls, and Cs)

clc;
clear all;

warning off;

f_points = (1:1:60)*1e3;          % switching frequency
Q = [0.1 0.2 0.5 0.8 1 2 5 8 10];
% Constants
Rac = 10.81;           % Resistance load viewed from the primary side
Rac1 = 0.155;         %Resistance load viewed from the secondary side
fr = 100e3;            % Resonant frequency
lambda = 0.0907;
Vin = 400;
vout = zeros(length(f_points),1);
for l = 1:length(Q)

    Z0 = Q(l)*Rac;
    Z01 = Q(l)*Rac1;
    Cp = 1/(2*pi*fr*Z0);
    Lp = Z0/(2*pi*fr);
    Cs = 1/(2*pi*fr*Z01);
    Ls = Z01/(2*pi*fr);

    fprintf('\n========= Simulation with Q = %f ==============\n',Q(l))
    fprintf('\n Lp = %0.01f uH , Cp = %0.01f uF, Ls = %0.01f uH , Cs =
            %0.01f uF \n', Lp*1e6, Cp*1e6, Ls*1e6, Cs*1e6);
    for k = 1:length(f_points)
        fin = f_points(k);
        sim('Full_gain.slx');
        vout(k) = data(end);

        fprintf('\n simulation %d out of %d done....\n',k,length(f_points))
    end
    plot(f_points/fr,vout/Vin,'linewidth',2); grid on; hold all;
end
%% Plot Data
legend(num2str(Q(1:end)'));
xlabel('f_s/f_r'); ylabel('V_o/V_{in}');

disp('Dear DC_DC LLC converter, Plotting successfully completed!!!!!');
```

Appendix A2

```
%% The general code developed to generates
% value for the parameter of the resonant tank
% (i.e. Lp, Cp, Ls, and Cs)

clear all;

warning off;

f_points = (1:1:60)*1e3;          % switching frequency
Q = [0.1 0.2 0.5 0.8 1 2 5 8 10];
% Constants
Rac = 10.81;           % Resistance load viewed from the primary side
Rac1 = 0.155;         %Resistance load viewed from the secondary side
fr = 100e3;            % Resonant frequency
Vin = 400;
vout = zeros(length(f_points),1);
for l = 1:length(Q)

    Z0 = Q(l)*Rac;
    Z01 = Q(l)*Rac1;
    Cp = 1/(2*pi*fr*Z0);
    Lp = Z0/(2*pi*fr);
    Cs = 1/(2*pi*fr*Z01);
    Ls = Z01/(2*pi*fr);

    fprintf('\n========== Simulation with Q = %f ==============\n', Q(l))
    fprintf(''\n Lp = %0.01f uH , Cp = %0.01f uF, Ls = %0.01f uH , Cs =
            %0.01f uF \n', Lp*1e6, Cp*1e6, Ls*1e6, Cs*1e6);
    for k = 1:length(f_points)
        fin = f_points(k);
        sim('Full_gain.slx');
        vout(k) = data(end);

        fprintf('\n simulation %d out of %d done....\n',k,length(f_points))
    end
    plot(f_points/fr, vout/Vin,'linewidth',2); grid on; hold all;
end
%% Plot Data
legend(num2str(Q(1:end)'));
xlabel('f_s/f_r'); ylabel('V_o/V_{in}');

disp('Dear DC_DC LLC converter, Plotting successfully completed!!!!!');
```

Appendix A3

```
%% The general code developed to generates
% value for the parameter of the resonant tank
% (i.e. Lp, Lmp, Cp, Ls, Lms, and Cs)

clc;
clear all;

warning off;

f_points = (1:1:60)*1e3;          % switching frequency
Q = [0.1 0.2 0.5 0.8 1 2 5 8 10];
% Constants
Rac = 10.81;           % Reaistance load veiwed from the primary side
Rac1 = 0.155;         %Reaistance load veiwed from the secondary side
fr = 100e3;            % Resonant frequency
lambda = 0.0907;
Vin = 400;
vout = zeros(length(f_points),1);
for l = 1:length(Q)

    Z0 = Q(l)*Rac;
    Z01 = Q(l)*Rac1;
    Cp = 1/(2*pi*fr*Z0);
    Lp = Z0/(2*pi*fr);
    Lmp = Lp/lambda;
    Cs = 1/(2*pi*fr*Z01);
    Ls = Z01/(2*pi*fr);
    Lms = Ls/lambda;

    fprintf('\n========== Simulation with Q = %f ==============\n',Q(l))
    fprintf('\n Lp = %0.01f uH , Cp = %0.01f uF, Ls = %0.01f uH , Lms =
            %0.01f uH Lmp = %0.01f uH Cs = %0.01f uF \n', Lp*1e6, Cp*1e6,
            Ls*1e6, Cs*1e6, Lmp*1e6, Lms*1e6);
    for k = 1:length(f_points)
        fin = f_points(k);
        sim('Full_gain.slx');
        vout(k) = data(end);

        fprintf('\n simulation %d out of %d done....\n',k,length(f_points))
    end
    plot(f_points/fr,vout/Vin,'linewidth',2); grid on; hold all;
end
%% Plot Data
legend(num2str(Q(1:end)'));
xlabel('f_s/f_r'); ylabel('V_o/V_{in}');

disp('Dear DC_DC LLC converter, Plotting successfully completed!!!!!');
```

Appendix C

The figure illustrates the zeros and poles of the plant that is found using MATLAB command pzmap(G_p). From the pole-zero map the system is stable all of its poles are less than zero values.

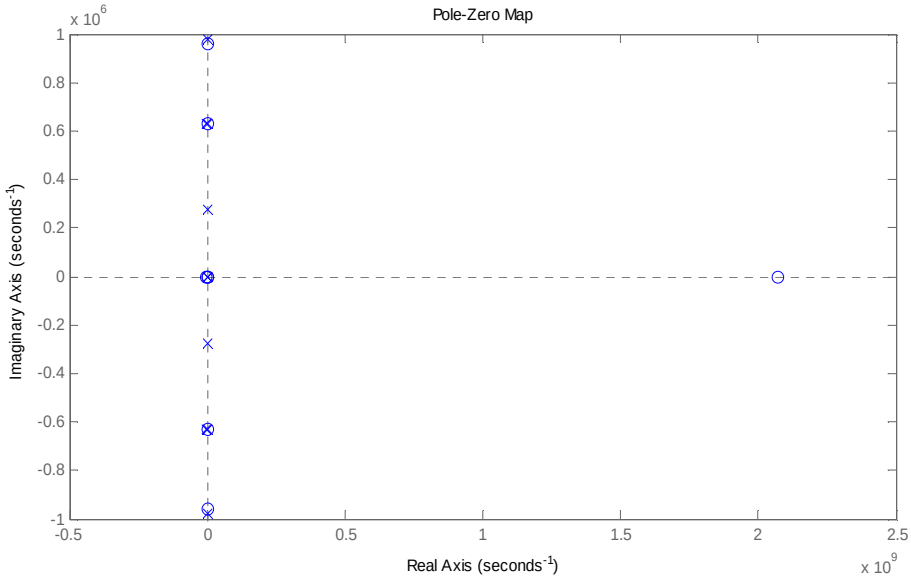

Body plot is used to determine the frequency response the LLC resonant converter. The ideal body bloat of the control to output transfer function as shown in the figure 11 is developed from the plant transfer function using the MATLAB command #bode(G_p). The theoretical body plot shows the open loop frequency response for the open loop of the resonant converter transfer function.

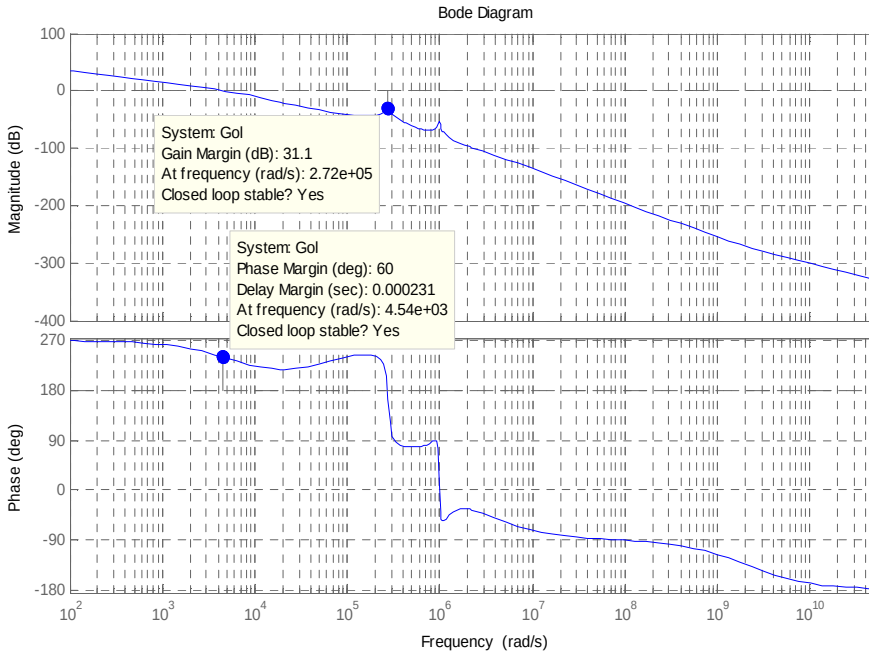
Bode Diagram
System: Gol
Gain Margin (dB): 31.1
At frequency (rad/s): 2.72e+05
Closed loop stable? Yes
System: Gol
Phase Margin (deg): 60
Delay Margin (sec): 0.000231
At frequency (rad/s): 4.54e+03
Closed loop stable? Yes
Magnitude (dB)
Phase (deg)
Frequency (rad/s)

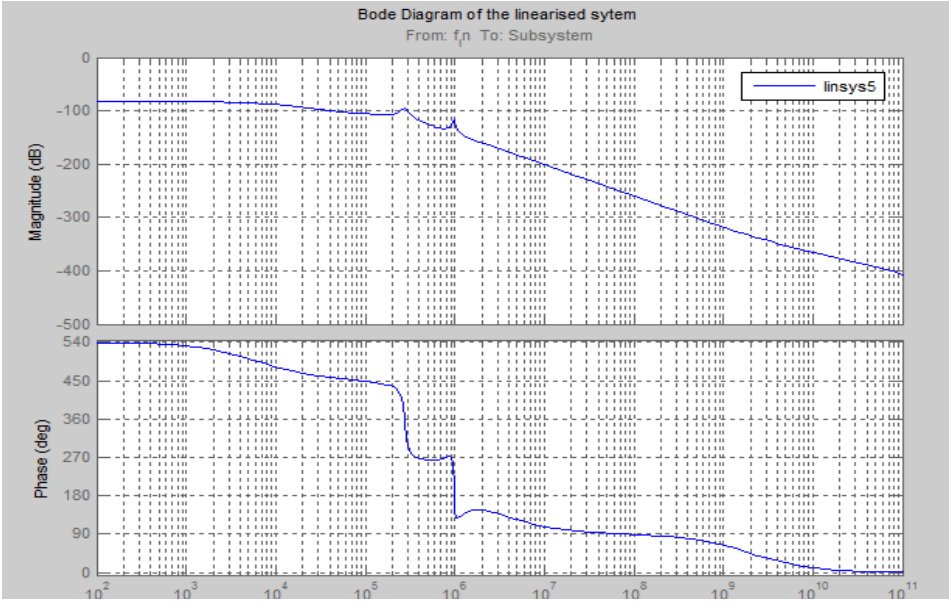
Bode Diagram of the linearised sytem
From: f_n To: Subsystem
linsys5
Magnitude (dB)
Phase (deg)

From equation 35, 36 and 37 the closed loop transfer function is analyzed as follows.

$$R = H_{cL}(s) = \frac{H_P * H_C}{1 + H_p H_c H_F}$$

The closed loop transfer function of the whole system provides information on the corner frequency due to the voltage sensor, zero and crossover of the inner current loop. While the open loop transfer function determines how the system responds to dc signal input because the reference signal is dc, the open loop gain provides information on the overall system stability.

Figure 12 shows bode plot diagram of the closed loop.

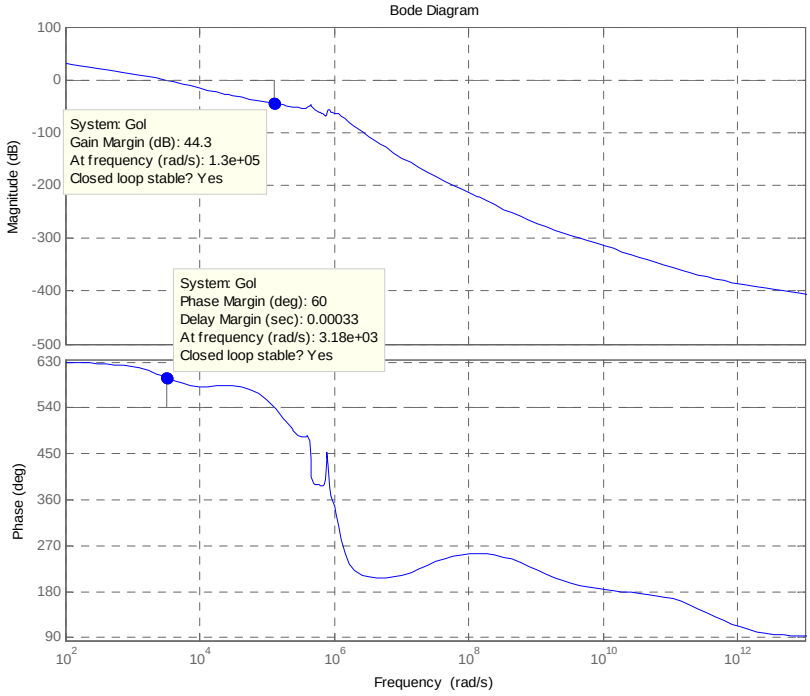

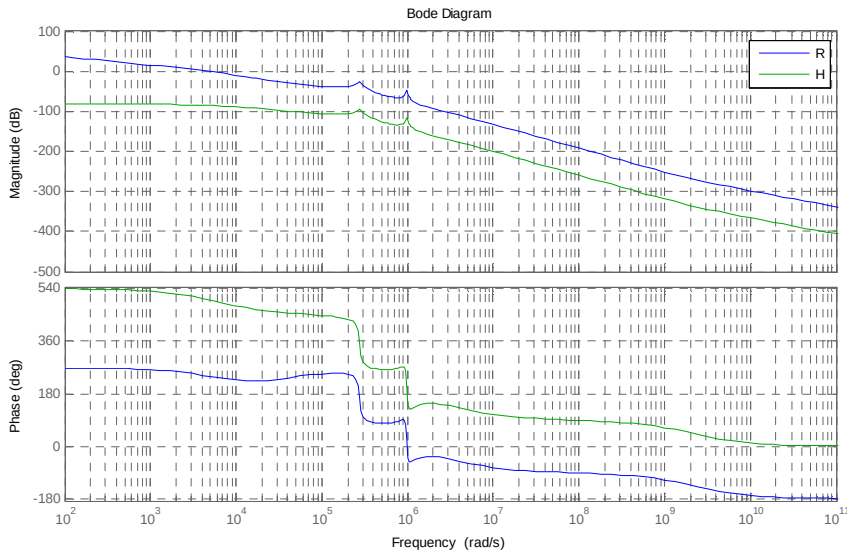

Fig 12: Bode diagram of loop gain

R: stands for the BP loop gain and H: Stands for BP of the resonant plant only ;

Appendix D

The simulink component of the converter are captured in detail as the following figures.

D1 The whole converter system including the controller, sensor and noise filter

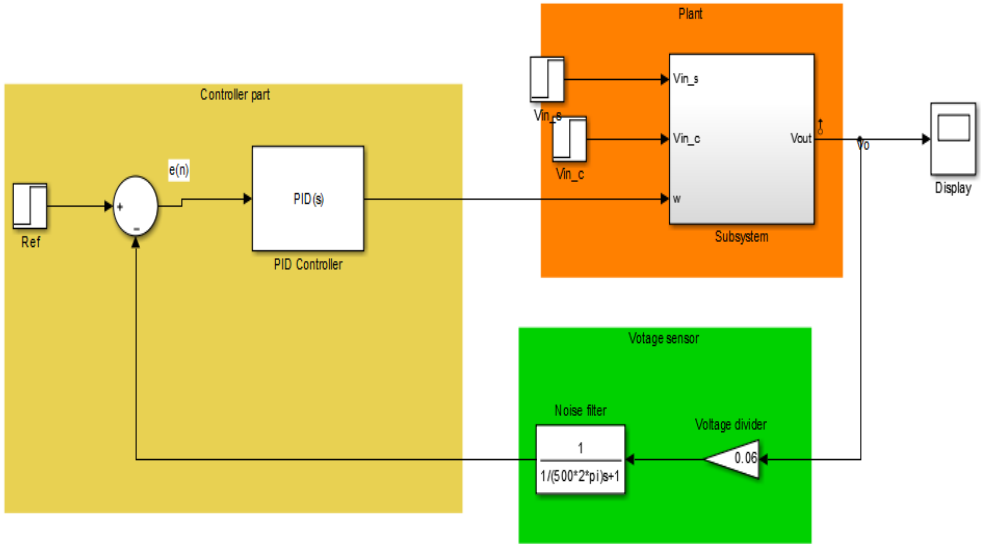

D2 Plant of the converter

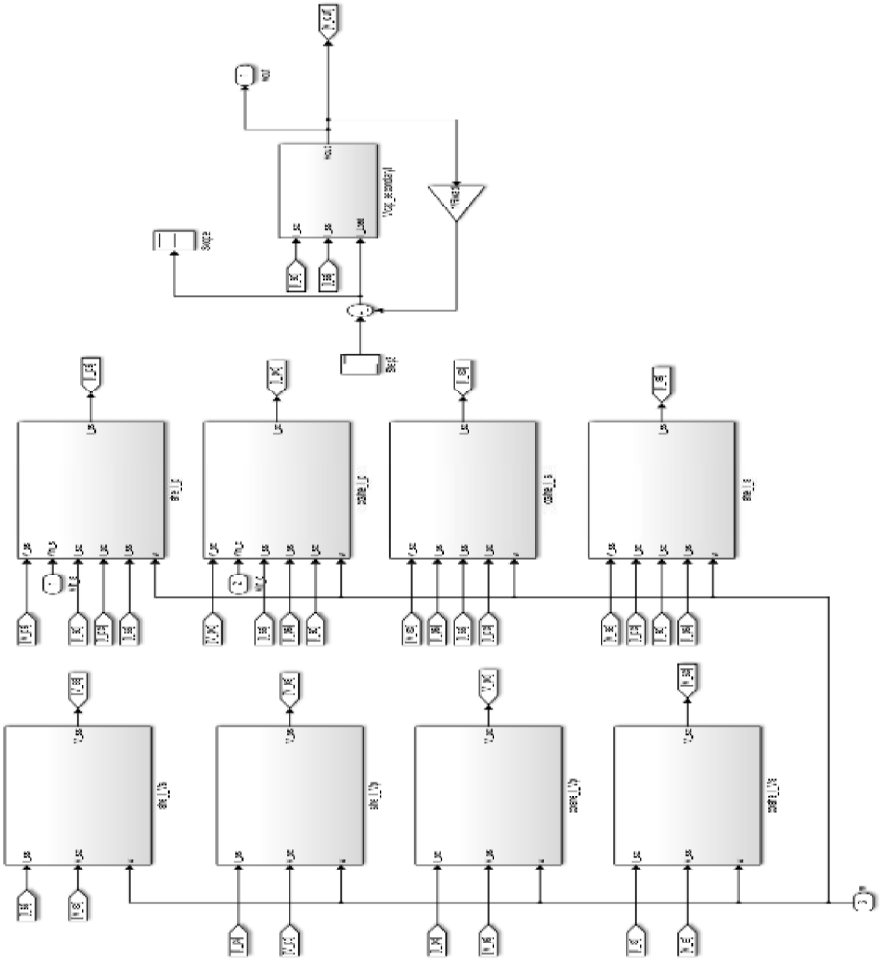

D3: sine component V_p-subsystem

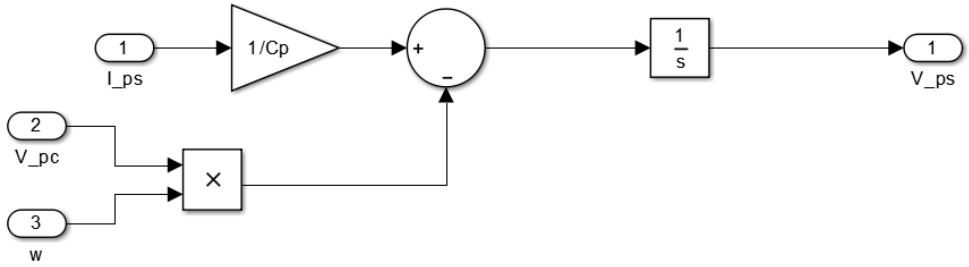

D4: cosine component V_p-subsystem

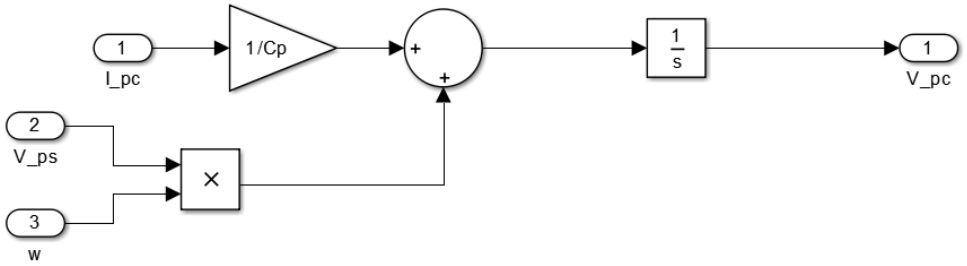

D5: sine component V_s-subsystem

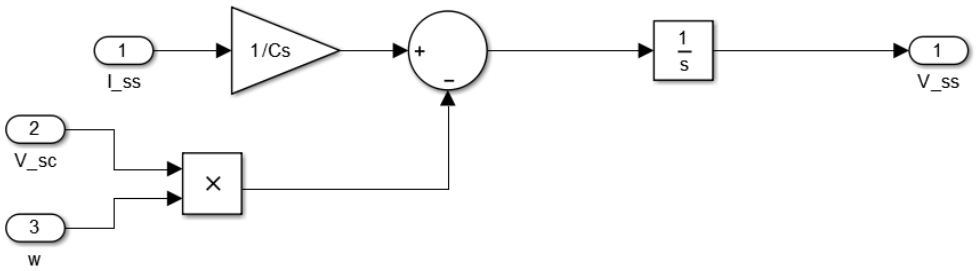

D6: cosine component V_s-subsystem

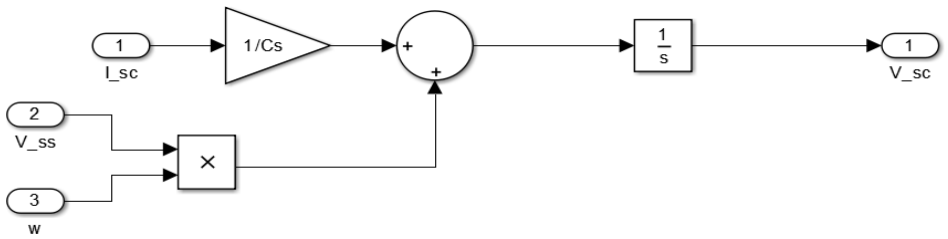

D7: sine component I_P-subsystem

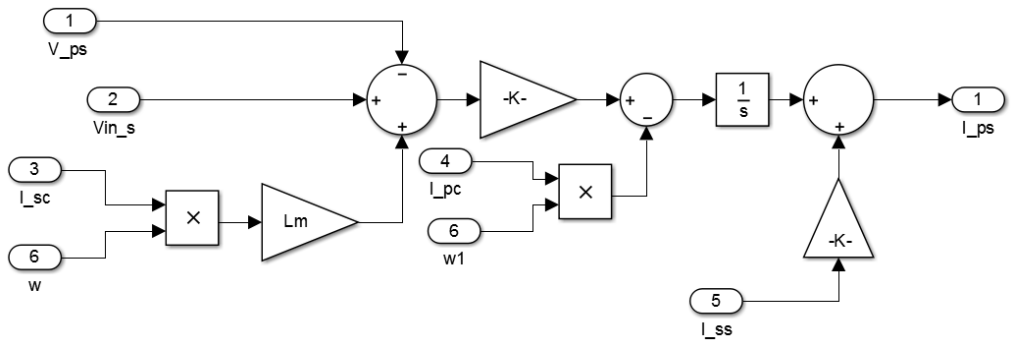

D8: cosine component I_P-subsystem

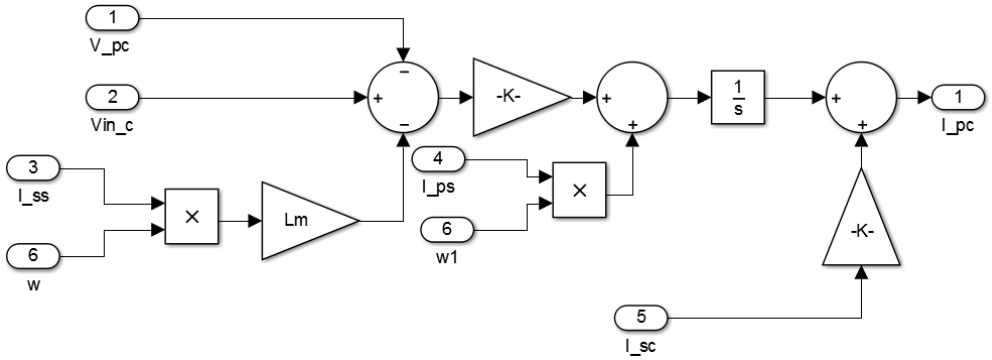

D9: sine component I_s subsystem

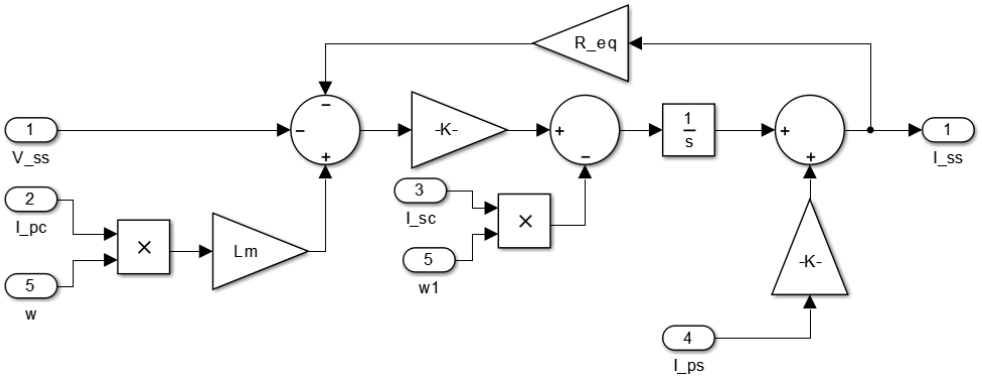

D10: cosine component of I_s subsystem

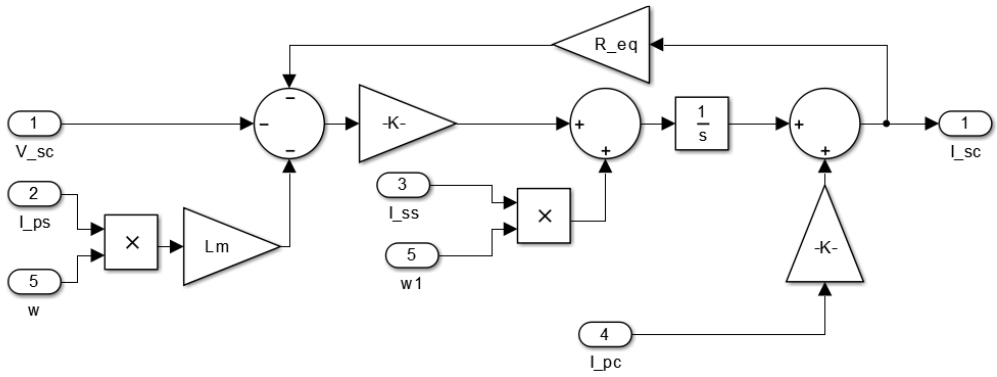

D11: Voltage on the capacitor on the output-side subsystem

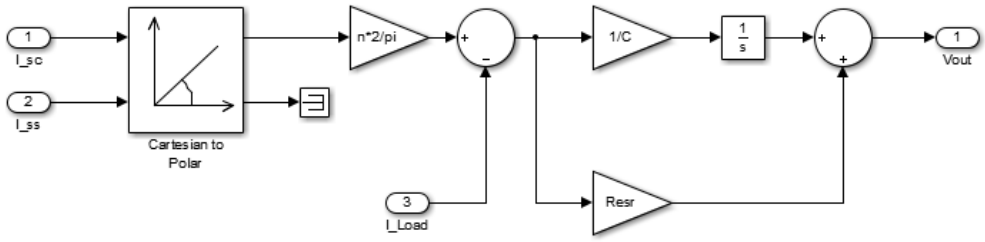

E PRINT CIRCUIT BOARD(PCB)

E1 Top View of the PCB

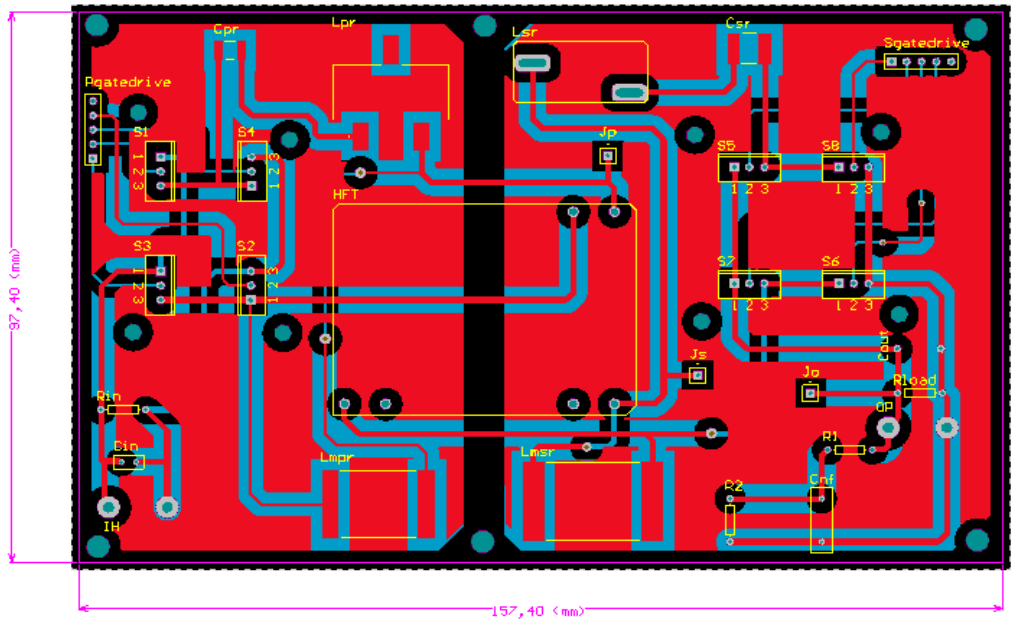

E1 Bottom View of the PCB